

**NATURAL-CONVECTION HEAT TRANSFER  
IN SUPERCRITICAL FLUIDS**

by

**Rolando A. Carreño Chávez**

A thesis submitted in partial fulfillment  
of the requirements for the degree of

**MASTER OF SCIENCE**

in

**MECHANICAL ENGINEERING**

**UNIVERSITY OF PUERTO RICO  
MAYAGÜEZ CAMPUS  
2004**

Approved by:

  
Sandra Coutín, Ph.D.  
Member, Graduate Committee

May 10, 2004  
Date

  
Nellore Venkataraman, Ph.D.  
Member, Graduate Committee

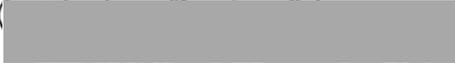
May 10, 2004  
Date

  
L. Antonio Estévez, Ph. D.  
President, Graduate Committee

May 10, 2004  
Date

  
Paul Sundaram, Ph.D.  
Chairperson of the Department

5/10/04  
Date

  
David Suleiman, Ph. D.  
Representative of Graduate Studies

5/10/04  
Date

## ABSTRACT

The main objective of this study is to calculate the heat-transfer coefficients for natural convection from a heated, vertical flat plate into a supercritical fluid. In the first part of this work, an equation for the coefficient of thermal expansion or expansivity for a van der Waals gas was derived as a function of the temperature, the pressure, the van der Waals constants, and the compressibility factor. The trend of the curves obtained with this equation and with values from tables of thermodynamic properties was similar and they diverge at critical point. These features confirm the validity of equation obtained in this work.

In the second part, this expansivity was used in the momentum equation, which, with the energy and continuity equation, forms a set of coupled equations. This set of equations was solved numerically by finite differences. A FORTRAN code was written to obtain the velocity and temperature profiles along the plate. The local Nusselt number was then calculated and plotted as a function of the local Rayleigh number. It is observed in these plots that a curve obtained with temperature and pressure far from the critical region approaches the line obtained with a classic correlation. It was also observed that the curves corresponding to supercritical conditions are notably above of the line corresponding to the classic correlation, which means that the heat transfer considerably increases in the critical region.

## RESUMEN

El objetivo principal de este estudio es calcular los coeficientes de transferencia de calor por convección natural para una placa plana vertical en contacto con un fluido supercrítico. En la primera parte de este trabajo se derivó una ecuación para el coeficiente de expansión térmica o expansividad para un gas de van der Waals en función de la temperatura, la presión, las constantes de van der Waals y el factor de compresibilidad. La tendencia de las curvas obtenidas con la ecuación calculada y valores de tablas de propiedades termodinámicas es la misma y ellas divergen en el punto crítico. Estas características confirman la validez de la ecuación obtenida en este trabajo.

En la segunda parte, esta expansividad se usó en la ecuación de movimiento que, con las ecuaciones de energía y continuidad, forma un sistema de ecuaciones acopladas. Este sistema de ecuaciones se resolvió numéricamente por diferencias finitas. Se escribió un programa FORTRAN para obtener los perfiles de velocidad y temperatura a lo largo de la placa. Se calculó el número de Nusselt local y se graficó en función del número de Rayleigh local. En los gráficos se observa que la curva obtenida con temperatura y presión lejos de la región crítica se aproxima a la línea obtenida con una correlación clásica. También se observó que las curvas correspondientes a condiciones supercríticas quedan notablemente por encima de la línea correspondiente a la correlación clásica lo que significa que la transferencia de calor aumenta considerablemente en la región crítica.

## **DEDICATION**

To my parents for their immeasurable support and love.

## ACKNOWLEDGMENTS

Looking back during the last two and half years when beginning this project, I remember that I had nothing in my hands; only the desires and enthusiasm to make something new. Now, after ups, downs, successes, failures, thrills, discoveries, and the like; the complete project can be seen with the prospective results and also not prospective. The M.Sc. experience, as a whole, has been very positive. This has been so because of many people that influenced my work, and my life during my stay in Mayagüez. I want to take this opportunity to thank them all.

First of all, I thank my advisor, Dr. L. Antonio Estévez, for his encouragement, support, and guidance in the development of this thesis. I consider myself fortunate to be his student. I would like also thank the Department of Mechanical Engineering, University of Puerto Rico, Mayagüez Campus for offering me a teaching assistantship during the first two years and the Department of General Engineering for offering graduate assistantship in this last year.

I wish to express my sense of gratitude and thanks to Dr. Gustavo Gutiérrez for their generous help in the second part of this thesis with the numerical code when I most needed it. I also thank Dr. Moses Bogere for their invaluable suggestions.

My special thanks are due to my friends Ezequiel Medici, for his support in my first programming attempt, using Matlab, and to Guillermo Araya for his help and suggestions while programming the final code in FORTRAN.

Finally, I must thank my parents and brothers, for their font love and all the support during various stages of my life.

## TABLE OF CONTENTS

LIST OF TABLES .....	x
LIST OF FIGURES .....	xi
LIST OF SYMBOLS .....	xiv
<b>CHAPTER 1. INTRODUCTION</b> .....	1
1.1 Background .....	1
1.2 Goals and Objectives .....	5
<b>CHAPTER 2. PREVIOUS WORK</b> .....	7
<b>CHAPTER 3. THERMODYNAMIC MODELING</b> .....	11
3.1 General Equation for Thermal Expansivity .....	11
3.2 Equation-of-State Approach .....	12
<b>CHAPTER 4. NATURAL CONVECTION EQUATIONS</b> .....	15
4.1 Heat Transport by Natural Convection .....	15
4.2 Boundary-Layer Equations for a Vertical Flat Plate.....	16
4.3 Heat-Transfer Coefficient .....	20
<b>CHAPTER 5. NUMERICAL SOLUTION</b> .....	21
5.1 Introduction .....	21
5.2 Numerical Model .....	21
5.2.1 Method of Finite-Differences.....	21
5.2.2 Description of the Solution Grid .....	22
5.2.3 Boundary-Layer Equations in Dimensionless Form .....	22

5.2.4 Finite-Difference Equations .....	25
5.2.5 Thomas Algorithm to Solve a Tridiagonal System of Equations .....	32
5.2.6 Relaxation Technique.....	35
5.3 Calculation of the Heat-Transfer Coefficient.....	36
5.4 Program Description .....	36
<b>CHAPTER 6. ESTIMATION OF FLUID PROPERTIES AND DESIGN OF</b>	
<b>    RUNS.....</b>	<b>44</b>
6.1 Fluids Selected .....	44
6.2 Design of Runs.....	45
6.3 Viscosity Estimation .....	46
6.4 Thermal Conductivity .....	48
6.5 Heat Capacity.....	50
<b>CHAPTER 7. RESULTS AND DISCUSSION.....</b>	
7.1 Thermodynamic Analysis .....	54
7.1.1 Reference Values for $\beta$ .....	54
7.1.2 Results .....	55
7.2 Heat Transport by Natural Convection .....	63
7.2.1 Grid Convergence Tests.....	63
7.2.2 Literature Correlation.....	65
7.2.3 Results.....	69

<b>CHAPTER 8. CLOSURE</b> .....	78
8.1 Conclusions.....	78
8.1.1 Thermodynamic Model.....	78
8.1.2 Numerical Model .....	79
8.2 Suggestions for Future Work .....	80
<b>BIBLIOGRAPHY</b> .....	81
APPENDIX A: Analytical Solution for Cubic Polynomial Equations .....	84
APPENDIX B: Heat Capacity .....	85
APPENDIX C: Numerical Code.....	86

## LIST OF TABLES

Table 1.1. Critical properties of some compounds used as supercritical solvents.....	3
Table 2.1. Summary of previous work.....	10
Table 6.1. Critical parameters of the fluids using for program running .....	44
Table 6.2. Inverse viscosity.....	47
Table 6.3. Dynamics Viscosity for the fluids near to the critical point .....	47
Table 6.4. Low-pressure thermal conductivity of the gas.....	49
Table 6.5. Constants to calculate the isobaric heat capacity .....	51
Table 6.6. Heat capacities for carbon dioxide.....	52
Table 6.7. Heat capacities for the butane .....	52
Table 6.8. Heat capacities for the water.....	53
Table 7.1 Bibliography used for tabulated densities.....	55
Table 7.2. Results of the temperature variation with the grid points .....	64
Table 7.3. Prandtl number for analytical equation.....	65

## LIST OF FIGURES

Figure 1.1. Phase diagram for a single component .....	3
Figure 4.1. Heated vertical plate .....	16
Figure 5.1. Grid used in the numerical solution.....	23
Figure 5.2. Grid points used to derive the finite-difference equations.....	25
Figure 5.3. Nodal points for the discretizing of the continuity equation .....	31
Figure 5.4. General flowchart of the program.....	37
Figure 5.5. Flowchart for subroutine ZETA .....	40
Figure 5.6. Flowchart for subroutine CALCBETA.....	41
Figure 5.7. Flowchart for subroutine TRISOL.....	42
Figure 6.1. Points in the supercritical region for the simulation analysis .....	45
Figure 7.1. Thermal expansion coefficient of carbon dioxide at 3.69 MPa.....	57
Figure 7.2. Thermal expansion coefficient of carbon dioxide at critical pressure (7.38 MPa) .....	57
Figure 7.3. Thermal expansion coefficient of carbon dioxide at 10.00 MPa.....	58
Figure 7.4. Thermal expansion coefficient of carbon dioxide at various pressures..... .....	58
Figure 7.5. Thermal expansion coefficient of butane at 1.80 MPa .....	59
Figure 7.6. Thermal expansion coefficient of butane at critical pressure .....	59
(3.796 MPa) .....	59
Figure 7.7. Thermal expansion coefficient of butane at 5.50 MPa .....	60

Figure 7.8. Thermal expansion coefficient of butane at various pressures .....	60
Figure 7.9. Thermal expansion coefficient of water at 11.045 MPa.....	61
Figure 7.10. Thermal expansion coefficient of water at critical pressure (22.09 MPa) .....	61
Figure 7.11. Thermal expansion coefficient of water at 33.135 MPa.....	62
Figure 7.12. Thermal expansion coefficient of water at various pressures.....	62
Figure 7.13. $Nu_x$ as a function of $Ra_x$ for carbon dioxide at $P_r = 1.05$ .....	71
Figure 7.14. $Nu_x$ as a function of $Ra_x$ for butane at $P_r = 1.05$ .....	71
Figure 7.15. $Nu_x$ as a function of $Ra_x$ for water at $P_r = 1.05$ .....	72
Figure 7.16. $Nu_x$ as a function of $Ra_x$ for carbon dioxide at $T_r = 1.05$ .....	73
Figure 7.17. $Nu_x$ as a function of $Ra_x$ for butane at $T_r = 1.05$ .....	73
Figure 7.18. $Nu_x$ as a function of $Ra_x$ for water at $T_r = 1.05$ .....	74
Figure 7.19. Dimensional velocity profile for water at $x = 0.02176$ [m], $P_r = 1.05$ , and $T_r = 1.05$ .....	75
Figure 7.20. Dimensional temperature profile for water at $x = 0.02176$ [m], $P_r = 1.05$ , and $T_r = 1.05$ .....	76
Figure 7.21. Velocity contour line for water at $P_r = 1.05$ and $T_r = 1.05$ .....	77
Figure 7.22. Temperature contour lines for water at $P_r = 1.05$ and $T_r = 1.05$ .....	77
Figure B.1. Inverse of the heat capacity of carbon dioxide as a function of reduced pressure and temperatures .....	86

Figure B.2. Inverse of the heat capacity of butane as a function of reduced pressure and temperatures .....	87
Figure B.3. Inverse of the heat capacity of water as a function of reduced pressure and temperatures .....	87

## LIST OF SYMBOLS

### Roman Symbols

$a$	EOS constant that corrects for intermolecular attractive forces, [ $\text{N}\cdot\text{m}^4/\text{mol}^2$ ]
$A$	Dimensionless EOS parameter, [-]
$A_c$	Dimensionless EOS parameter $A$ evaluated at the critical point, [-]
$A'$	Heat-transfer area, [ $\text{m}^2$ ]
$b$	EOS constant that corrects for volume of gas molecules, [ $\text{m}^3/\text{mol}$ ]
$B$	Dimensionless EOS parameter, [-]
$B_c$	Dimensionless EOS parameter $B$ evaluated at the critical point, [-]
$C$	Dimensionless parameter, [-]
$C_j$	Dimensionless coefficient in the momentum equation, [-]
$C_p$	Heat capacity of the fluid, [ $\text{J}/\text{kg}\cdot\text{K}$ ]
$C_p^0$	Heat capacity at the low-pressure limit, [ $\text{J}/\text{kg}\cdot\text{K}$ ]
$D_j$	Dimensionless coefficient in the momentum equation, [-]
$E_j$	Dimensionless coefficient in the momentum equation, [-]
$F_j$	Dimensionless coefficient in the momentum equation, [-]
$g$	Local acceleration of gravity, [ $\text{m}/\text{s}^2$ ]
$G^\circ$	Dimensionless coefficient, [-]
$G_j$	Dimensionless coefficient in the energy equation, [-]
$\text{Gr}_w$	Grashof number, [-]

$h_x$	Local heat-transfer coefficient, [W/m <sup>2</sup> ·K]
$\bar{h}_L$	Average heat-transfer coefficient, [W/m <sup>2</sup> ·K]
$H_j$	Dimensionless coefficient in the energy equation, [-]
$J_j$	Dimensionless coefficient in the energy equation, [-]
$k$	Thermal conductivity of the fluid, [W/m·K]
$k^0$	Thermal conductivity at the low-pressure limit, [W/m·K]
$L$	Height of the vertical plate (length in the $x$ direction), [m]
$m$	Dimensionless parameter, [-]
$M$	Molecular weight of the fluid, [kg/mol]
$n$	Dimensionless parameter, [-]
$N$	Number of lines parallel to the $x$ direction, [-]
$\overline{\text{Nu}}_L$	Average Nusselt number, [-]
$\text{Nu}_x$	Local Nusselt number, [-]
$P$	Pressure, [Pa]
$P_c$	Critical pressure, [Pa]
$P_r$	Reduced pressure, [-]
$\text{Pr}$	Prandtl number, [-]
$q_c$	Convective heat transfer, [W/m <sup>2</sup> ]
$q_k$	Conduction heat transfer, [W/m <sup>2</sup> ]
$R$	Gas constant, [J/mol·K]
$\text{Ra}_L$	Rayleigh number for the whole plate, [-]

$S_j$	Dimensionless coefficient in the energy equation, [-]
$T$	Temperature, [K]
$T_c$	Critical temperature, [K]
$T_f$	Fluid average temperature, [K]
$T_r$	Reduced temperature, [-]
$T_w$	Wall temperature of the vertical flat plate, [K]
$T_\infty$	Fluid medium temperature (outside the boundary layer), [K]
$u'$	EOS parameter, [-]
$u$	Velocity component in the $x$ direction, [m/s]
$U$	Dimensionless velocity component in the $x$ direction, [-]
$v$	Velocity component in the $y$ direction, [m/s]
$V$	Dimensionless velocity component in the $y$ direction, [-]
$V'$	Molar volume, [m <sup>3</sup> /mol]
$V_c$	Critical molar volume, [m <sup>3</sup> /mol]
$w$	EOS parameter, [-]
$W$	Width of the solution domain (in the $y$ direction), [m]
$x$	Coordinate parallel to the vertical plate, [m]
$X$	Dimensionless coordinate parallel to the vertical plate, [-]
$X_{max}$	Dimensionless length of the vertical plate, [-]
$y$	Coordinate normal to the vertical plate, [m]
$Y$	Dimensionless coordinate perpendicular to the vertical plate, [-]

$Z$	Compressibility factor, [-]
$Z_c$	Critical compressibility factor, [-]

### **Greek Symbols**

$\alpha$	Thermal diffusivity, [m <sup>2</sup> /s]
$\alpha'_j$	Dimensionless parameter, [-]
$\beta$	Thermal expansivity or thermal expansion coefficient, [1/K]
$\beta_i$	Ideal-gas thermal expansivity coefficient, [1/K]
$\beta_{ref}$	Reference value of the thermal expansivity, [1/K]
$\beta^*$	Dimensionless thermal expansivity, [-]
$\gamma$	Kinematic viscosity, [m <sup>2</sup> /s]
$\Gamma$	Inverse thermal conductivity, [m·K/W]
$\Delta T$	Difference between the wall temperature and the fluid temperature [K]
$\Delta T_r$	Reduced temperature variation [-]
$\Delta x$	Dimensional step size of the grid in the $x$ direction, [m]
$\Delta X$	Dimensionless step size of the grid in the $x$ direction, [-]
$\Delta X_{max}$	Highest dimensionless step size of the grid in the $x$ direction, [-]
$\Delta y$	Dimensional step size of the grid in the $y$ direction, [m]
$\Delta Y$	Dimensionless step size of the grid in the $y$ direction, [-]
$\eta$	Dynamic viscosity, [Pa·s]
$\theta$	Dimensionless temperature, [-]

$\xi$	Inverse viscosity, [ $\text{m}^2/\text{N}\cdot\text{s}$ ]
$\rho$	Density of the fluid, [ $\text{kg}/\text{m}^3$ ]
$\rho^*$	Ideal-gas fluid density (low-pressure limit), [ $\text{kg}/\text{m}^3$ ]
$\rho_\infty$	Density of the fluid outside the boundary layer, [ $\text{kg}/\text{m}^3$ ]
$\rho_r$	Reduced density, [-]
$\rho'_j$	Dimensionless parameter, [-]
$\phi_j$	Dimensionless parameter, [-]
$\psi_j$	Dimensionless parameter, [-]
$\omega$	Acentric factor, [-]

### Subscripts

$i$	Node in the $x$ direction
$j$	Node in the $y$ direction
$P$	Constant pressure
$\infty$	Outside the boundary layer

### Abbreviations

EOS	Equations of state
SCF	Supercritical fluid
SFE	Supercritical fluid extraction

# CHAPTER 1

## INTRODUCTION

### 1.1 Background

The application of the supercritical fluids in the industry has attracted a great deal of attention due to the broad range of applications and low or negligible environmental impact. Numerous vegetable and animal substances have been processed with supercritical solvents to extract their valuable components. An important example is the extraction of essences of aromatic and medicinal plants, which have been carried out to a great extent with supercritical carbon dioxide.

It is well known that, at the critical point, the properties of the liquid and vapor phases become identical and cannot be distinguished. A supercritical fluid is a fluid at temperatures and pressures higher than the critical ones, as seen in Fig. 1.1. The critical properties of common fluids used for supercritical fluid extraction (SFE) processes are given in Table 1.1.

There is ample evidence that supercritical fluids provide an alternative to the use of conventional solvents to carry out a variety of processes. First, it is possible to use environmentally benign fluids as water, carbon dioxide (CO<sub>2</sub>), or other fluids that are not that environmentally friendly, such as ammonia or the low-molecular-weight hydrocarbons. Second, it is possible to harness the density by slight changes in pressure and thus adjusting its capacity as a dissolvent to optimize

their performance and selectivity in separation processes or in chemical reactions. Third, the moderate temperatures often used, as in the case of CO<sub>2</sub> or light hydrocarbons, are an additional advantage when dealing with labile substances commonly encountered in biotechnological applications.

The processes involving supercritical fluids are sometimes more expensive than the conventional processes because they involve high-pressure equipment. This is partially offset in many instances, i.e., when CO<sub>2</sub> is used, by the readily available and inexpensive solvent used.

For more than twenty years, supercritical solvents have been used in large-scale processes. One of the first processes was the extraction of caffeine from coffee beans with supercritical CO<sub>2</sub>. Supercritical extraction has also been used to extract substances such as hops and spices from plants. As stated previously, the cost associated with the compression and the confinement of the fluids at high pressure is what makes this technology costly, in many cases more than traditional methods. Nevertheless, the simplicity, the selectivity and the low or negligible environmental impact that supercritical-fluid technologies offers will progressively turn on important options, and in the future supercritical fluids will be probably used massively.

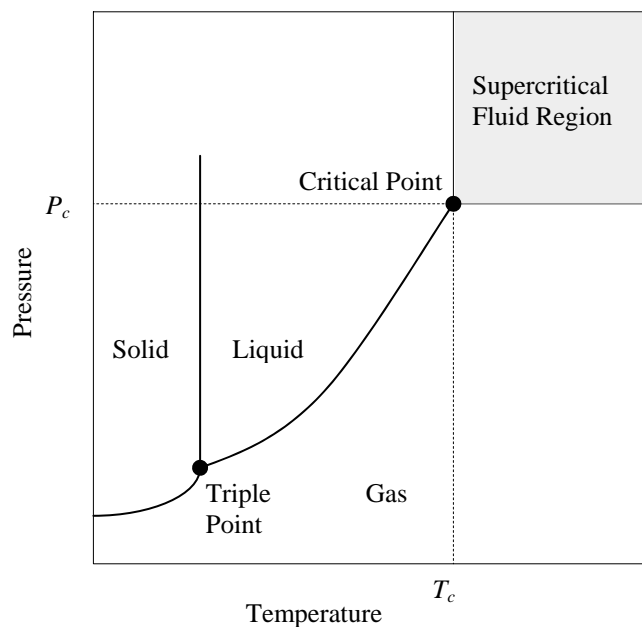


Figure 1.1. Phase diagram for a single component.

Table 1.1. Critical properties of some compounds used as supercritical solvents

Fluid	Critical Temperature [K]	Critical Pressure [MPa]
ammonia	405.50	11.35
butane	425.16	3.80
carbon dioxide	304.10	7.38
chlrorotrifluoromethane	302.00	3.87
cyclohexane	553.50	4.07
ethane	305.40	4.88
ethylene	282.40	5.04
n-pentane	469.70	3.37
propane	369.80	4.25
propylene	364.90	4.60
toluene	591.80	4.10
trichlorofluoromethane	471.20	4.41
trifluoromethane	299.30	4.86
water	647.30	22.09

The supercritical fluids have many unique advantages. Their diffusivity properties are much better than those of a liquid, allowing the supercritical fluid to penetrate into ultra fine nanostructures. They produce no capillary stress during the drying process due to the absence of a liquid-gas-interface. Also, SCF can be used for the extraction or removal of specific material from nanostructures.

Extraction is not the only application of supercritical fluids. In the petrochemical industry, supercritical fluids are used for the recovery of oil by flooding the wells with high-pressure CO<sub>2</sub>, which happens to be supercritical. Supercritical fluids are also used as a reaction medium in the cracking of the heavy components of petroleum with supercritical pentane and for the tar extraction with supercritical toluene. More recently, processes are being developed in the field of particle technology using supercritical fluids.

One of the first industrial, supercritical-extraction processes was the decaffeination of coffee beans, and this process will be used to illustrate the importance of the this investigation. To extract the caffeine from the coffee bean, an extractor with a heating jacket is used, inside which the coffee beans are placed and through which supercritical CO<sub>2</sub> circulates, forming a supercritical-fluid bed. The heat must flow from the heating jacket to the supercritical fluid and from there to the beans. The mechanism of heat transfer in the bed is very important. In this case mechanisms are forced convection, due to the circulation of supercritical CO<sub>2</sub>,

and natural convection due to the density variations. Müller and Estévez [16] found that, in the case of mass transfer, the natural convection is greatly increased when supercritical conditions are approached. Therefore, it would not be surprising to find out that natural-convection heat transfer would exhibit a similar behavior.

## **1.2 Goals and Objectives**

Given the important applications mentioned above, and the need to understand the relative importance of the heat-transfer mechanisms involved, it is the goal of this work to predict the enhancement of the natural heat-transfer phenomenon near the solvent critical point. This is done by obtaining a model to predict the natural convection heat-transfer coefficient that applies to the case where the medium is a supercritical fluid. To this end, a mathematical model was developed in two steps. First, a thermodynamic model based on a cubic equation of state was developed to estimate the thermal expansivity. The van der Waals equation was used to this end. Then, the boundary-layer, heat-transfer equations incorporating the dependence of the thermal expansivity on temperature were solved numerically to reach the desired model for the heat-transfer coefficient.

The specific problem used to search the main goal of this work involves heat transfer by natural convection to or from a solid vertical, flat plate, when the fluid medium is a supercritical fluid. The strategy chosen comprises the following steps:

1. Find a general equation for the thermal expansivity ( $\beta$ ) as a function of pressure and temperature using a cubic equation of state. Compute  $\beta$  in the vicinity of the critical point for a selected group of compounds that are or could be used as supercritical solvents.
2. Find the governing differential equations (continuity, motion, and energy) for the geometry at hand.
3. Find a numerical solution (temperature and velocity distribution) to the differential equations obtained in step 2, using a variable thermal expansivity calculated point to point from equation obtained in step 1.
4. Compute the heat-transfer coefficient for selected fluids, at preselected conditions according to a “design of experiments” method.
5. Correlate the results in terms of standard dimensionless numbers and compare it to standard correlations.

## CHAPTER 2

### PREVIOUS WORK

The heat transfer by natural convection applied to simple geometries such as flat plates, spheres, and cylinders, have been extensively studied for decades. Information on many topics related to supercritical-fluid technologies is also abundant. However, studies of natural convection in supercritical fluid are very scarce, suggesting that not much work has been done in this field.

The classical approach to mathematically describe natural convection for simple geometries is as follows. The energy equation and the Navier-Stokes equations are first stated and simplified for the particular geometry being studied. Then, the density of the fluid is expressed in terms of the thermal expansivity,  $\beta$ , (assumed constant) and the temperature and substituted into the Navier-Stokes equations. The resulting differential equations are coupled (because the temperature appears in the Navier-Stokes equations and the velocity components appear in the energy equation) and thus they are solved simultaneously. Once the temperature distribution is obtained, the heat-transfer coefficient is readily calculated.

Ostrach, [21] was one of the first to solve the boundary layer equations for natural convection from vertical flat plane using a numerical method, reducing the set of three equations (continuity, momentum and energy) to only two equations

with their respective boundary conditions. He found that this type of flow is dependent on the Grashof number and Prandtl number.

McHugh and Krukoni [14] gave an excellent introduction to the properties and uses of supercritical fluids. A good way to define a SCF is with a phase diagram that indicates the critical temperature and pressure of a substance. (For example, CO<sub>2</sub>;  $T_c = 304.10$  [K],  $P_c = 7.38$  [MPa]) Supercritical fluids are highly compressible and resemble gases in some aspects and liquids in others. Such fluids as supercritical xenon, ethane, and carbon dioxide offer a range of unusual possibilities in separation processes and in analytical or synthetic chemistry.

Müller and Estévez [16] made an important contribution to understanding mass transfer by natural convection in supercritical fluid. They modeled the isothermal-isobaric expansivity on mixing (analog of the thermal expansivity in heat transfer), through cubic equations of state for this case. They found that this expansivity gets to be quite high close to the critical point of the solvent. They also found that the dependency of this expansivity on composition is significant, reaching a maximum value at infinite dilution. It has been observed that the mass- and heat-transfer phenomena are analog in many aspects.

Therefore, if the value of expansivity found by Müller and Estévez [16] is high in the case of mass transfer, one would expect that the thermal expansivity  $\beta$  be also high under similar conditions based on mass and heat-transfer analogies.

Nishikawa and Ito [19] did modeling for free convection to supercritical fluids based on boundary-layer equations and similarity transformation taking into account variable physical properties of the fluid. However, no effect of the temperature on the thermal expansivity was accounted for. The same group also did experiments on free convection from thin wires [18]. Kakarala and Thomas [11], on the other hand, did some modeling for free and forced convection for flow of supercritical fluids in vertical tubes.

To the author's knowledge, no recent contributions on free convection in supercritical fluids have appeared in the literature. The works mentioned in this chapter are summarized in Table 2.1.

Table 2.1. Summary of previous work

Author	Type of work	Geometry or comment	Contribution
Ostrach (1952) [21]	Numerical solution	Heated vertical flat plate	Solve numerically the boundary layer equations with constant thermal expansivity
Nishikawa et al. (1973) [18]	Experiments	Wires	Measured heat flux from wires to supercritical CO <sub>2</sub>
Nishikawa and Ito (1969) [19]	Modeling	Vertical flat plate	Numerical solution with properties varying with temperature
Kakarala and Thomas (1980) [11]	Modeling of turbulent flow	Flow of SCF in tubes	Use surface renewal to model combined free and forced convection
Müller and Estévez (1990) [16]	Thermodynamic model	Mass-transfer natural convection	Model the isothermal-isobaric expansivity on mixing, through cubic equations of state
McHugh and Krukonis (1994) [14]	Introduction to supercritical fluids	Book on fundamentals and applications	Introduction to the properties and uses of the supercritical fluids
This work	Thermodynamic model and numerical solution	Heated vertical flat plate	Solve numerically the boundary layer equations with variable thermal expansivity

## CHAPTER 3

### THERMODYNAMIC MODELING

#### 3.1 General Equation for Thermal Expansivity

The analysis presented here begins with the definition of isobaric thermal expansivity  $\beta$  (or simply, thermal expansivity):

$$\beta = -\frac{1}{\rho} \left( \frac{\partial \rho}{\partial T} \right)_P \quad (3.1)$$

and expressing  $\rho$  as,

$$\rho = \frac{\rho^*}{Z} \quad (3.2)$$

where  $\rho^*$  is the ideal-gas fluid density at  $P$  and  $T$  and  $\rho$  is the actual density of the fluid at  $P$  and  $T$ . The derivative of Eq. (3.2) with respect to  $T$  at constant  $P$  is:

$$\left( \frac{\partial \rho}{\partial T} \right)_P = \left( \frac{\partial (\rho^* Z^{-1})}{\partial T} \right)_P = \frac{1}{Z} \left( \frac{\partial \rho^*}{\partial T} \right)_P - \frac{\rho^*}{Z^2} \left( \frac{\partial Z}{\partial T} \right)_P \quad (3.3)$$

Replacing Eq. (3.3) in Eq. (3.1) yields:

$$\begin{aligned} \beta &= -\frac{1}{\rho} \left( \frac{\partial \rho}{\partial T} \right)_P = -\frac{Z}{\rho^*} \left[ \frac{1}{Z} \left( \frac{\partial \rho^*}{\partial T} \right)_P - \frac{\rho^*}{Z^2} \left( \frac{\partial Z}{\partial T} \right)_P \right] \\ &= -\frac{1}{\rho^*} \left( \frac{\partial \rho^*}{\partial T} \right)_P + \frac{1}{Z} \left( \frac{\partial Z}{\partial T} \right)_P = \beta_i + \frac{1}{Z} \left( \frac{\partial Z}{\partial T} \right)_P = \frac{1}{T} + \frac{1}{Z} \left( \frac{\partial Z}{\partial T} \right)_P \end{aligned} \quad (3.4)$$

where  $\beta_i$  is the ideal-gas thermal expansivity, equal to  $1/T$ . Eq. (3.4) is completely general and applies to any material, in particular, dense fluids. It can be used whenever the relationship  $Z = Z(P, T)$  is known.

### 3.2 Equation-of-State Approach

Schmidt and Wenzel [25] present a general form for cubic equations of state (EOS). Their equation is suitable at high pressures and temperatures such as those encountered in processes with supercritical fluids. The equation is:

$$P = \frac{RT}{V'-b} - \frac{a}{V'^2 + u'bV' + wb^2}$$

(3.5)

The polynomial form of Eq. (3.5) is:

$$V'^3 P + V'^2 [Pb(u'-1) - RT] + V' [Pb^2(w-u') + a - u'RTb] - b[bw(Pb + RT) + a] = 0$$

(3.6)

To express Eq. (3.6) in terms of  $Z$ , the following definitions are recalled:

$$Z = \frac{PV'}{RT}$$

(3.7)

$$A = \frac{aP}{(RT)^2}$$

(3.8)

and

$$B = \frac{bP}{RT}$$

(3.9)

where  $a$  and  $b$  are the EOS constants normally obtained from the critical properties.

Replacing Eqs. (3.7), (3.8) and (3.9) into Eq. (3.6) yields, after rearrangement:

$$Z^3 + [(u'-1)B - 1]Z^2 + [A - u'B - B^2(u'-w)]Z - B(A + wB + wB^2) = 0$$

For van der Waals EOS:

$$u' = 0, \quad w = 0$$

Therefore, the polynomial equation is reduced to:

$$Z^3 - (B+1)Z^2 + AZ - AB = 0 \quad (3.10)$$

Moreover,

$$a = \frac{27}{64} \frac{(RT_c)^2}{P_c}$$

(3.11)

$$b = \frac{1}{8} \frac{RT_c}{P_c} \quad (3.12)$$

and, from Eqs. (3.8) and (3.9):

$$A_c = \frac{27}{64} = 0.421875 \quad B_c = \frac{1}{8} = 0.125$$

Equations (3.4) and (3.10) are the basis to obtain an expression for the thermal expansivity as a function of the pressure and temperature. The implicit derivative of Eq. (3.10) with respect to  $T$  a constant  $P$  is:

$$\left[ 3Z^2 - 2Z(B+1) + A \right] \left( \frac{\partial Z}{\partial T} \right)_P - (Z^2 + A) \left( \frac{\partial B}{\partial T} \right)_P + (Z - B) \left( \frac{\partial A}{\partial T} \right)_P = 0 \quad (3.13)$$

But, from Eqs. (3.8) and (3.9):

$$\left( \frac{\partial A}{\partial T} \right)_P = -\frac{2A}{T} \quad (3.14)$$

$$\left( \frac{\partial B}{\partial T} \right)_P = -\frac{B}{T} \quad (3.15)$$

Substituting Eqs. (3.14) and (3.15) into Eq. (3.13) yields:

$$\left(\frac{\partial Z}{\partial T}\right)_p = \frac{-Z^2 B + 2ZA - 3AB}{T(3Z^2 - 2Z(B+1) + A)} \quad (3.16)$$

subsequent substitution of Eq. (3.16) in Eq. (3.4), gives:

$$\beta = \frac{1}{T} \left[ 1 - \left( \frac{Z^2 B - 2ZA + 3AB}{3Z^3 - 2Z^2(B+1) + ZA} \right) \right] \quad (3.17)$$

This is an expression for  $\beta$  as a function of compressibility factor, pressure, and temperature. The calculation of  $\beta$  involves two steps: first, the compressibility factor,  $Z$ , is determined by finding the appropriate root of Eq. (3.10); then,  $Z$  is introduced into Eq. (3.17) to obtain the value of  $\beta$ . Equation (3.10) is a cubic equation and the procedure to find its roots is shown in Appendix A.

It is interesting to verify that Eq. (3.17) converges to  $1/T$  at the ideal-gas limit. This limit is reached as  $P \rightarrow 0$  at constant  $T$ . When this happens,  $PV' \rightarrow RT$ , i.e.,  $Z \rightarrow 1$ , (Eq. 3.7) and  $A \rightarrow 0$  and  $B \rightarrow 0$ , (Eqs. (3.8) and (3.9)). Therefore:

$$\beta = \frac{1}{T} \quad (3.18)$$

## CHAPTER 4

### NATURAL CONVECTION EQUATIONS

#### 4.1 Heat Transport by Natural Convection

In natural or free convective heat transfer, heat is transferred between a solid surface and a fluid moving over it, where fluid motion is entirely caused by the buoyancy forces arising from density changes that result from the temperature variations in the fluid. Fluid movement by natural convection can be either laminar or turbulent. However, because of the low velocities that usually exist in natural convection, laminar flow occurs more frequently than turbulent flow. In this thesis, attention will therefore be focused on laminar natural convective flow.

Fluid movement by free convection is due to density changes in the presence of a gravitational force field. It can also arise in other force fields, e.g., very large buoyancy in a centrifugal force field. However, in these cases, the movement is not normally purely natural convective. Such cases will not be considered here. A distinction is sometimes made between natural and free convection, the term natural convection then being applied to fluid movement caused by a gravitational force field and term free convection being applied to movement caused by any force field. However, current trend is to use either term to describe fluid flow caused by temperature-induced density changes in any force field and thus they will be used interchangeably here.

## 4.2 Boundary-Layer Equations for a Vertical Flat Plate

Consider the laminar boundary layer depicted in Fig. 4.1, where the fluid movement is entirely driven by buoyancy forces. In this two-dimensional problem, the gravity acts in the negative  $x$  direction. If the temperature differences are small enough, the fluid properties, except the fluid density, may be assumed to be constant (fluid density can not be assumed constant, because its variation is what induces the fluid motion). Finally, it will assumed that the boundary layer approximations are valid.

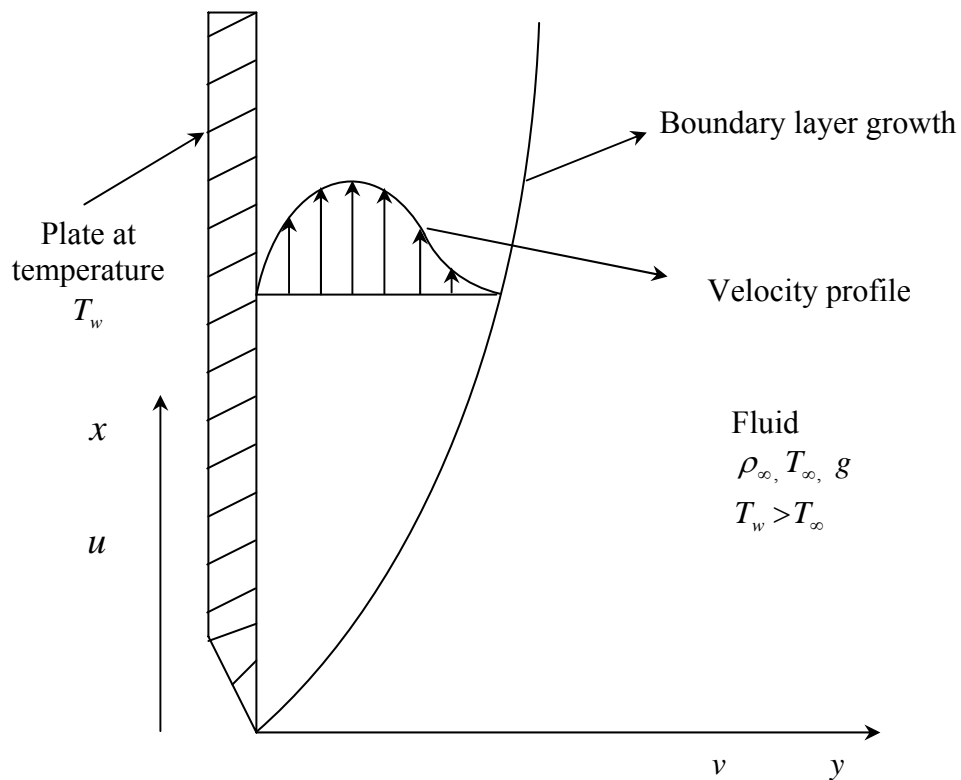


Figure 4.1. Heated vertical plate.

The body force by unit volume is  $-\rho g$ , where  $g$  is the local acceleration of gravity. Thus, momentum equation in the  $x$  direction is,

$$\rho \left( \frac{\partial u}{\partial t} + u \frac{\partial u}{\partial x} + v \frac{\partial u}{\partial y} \right) = -\frac{\partial P}{\partial x} + \eta \left( \frac{\partial^2 u}{\partial x^2} + \frac{\partial^2 u}{\partial y^2} \right) - \rho g \quad (4.1)$$

where,

$$\frac{\partial u}{\partial t} = 0 \quad (\text{Steady state})$$

$$\frac{\partial^2 u}{\partial y^2} \gg \frac{\partial^2 u}{\partial x^2} \quad (\text{Order-of-magnitude analysis})$$

Then, Eq. (4.1) becomes:

$$\rho \left( u \frac{\partial u}{\partial x} + v \frac{\partial u}{\partial y} \right) = -\frac{\partial P}{\partial x} + \eta \frac{\partial^2 u}{\partial y^2} - \rho g \quad (4.2)$$

The pressure gradients in the boundary layer correspond to hydrostatic effects of the fluid. Assuming that the pressure gradient inside and outside the boundary layer is the same, then:

$$\frac{\partial P}{\partial x} = -\rho_{\infty} g \quad (4.3)$$

where  $\rho_{\infty}$  is the density outside the boundary layer.

Replacing Eq. (4.3) in Eq. (4.2),

$$\rho \left( u \frac{\partial u}{\partial x} + v \frac{\partial u}{\partial y} \right) = g (\rho_{\infty} - \rho) + \eta \frac{\partial^2 u}{\partial y^2} \quad (4.4)$$

The first term on the right-hand side of Eq. (4.4) is the buoyancy force, where the density  $\rho$  is a variable. The density may be represented by a linear function of temperature for small temperature differences and the change in density is related to the thermal expansivity,  $\beta$ , as:

$$\beta = -\frac{1}{\rho} \left( \frac{\partial \rho}{\partial T} \right)_p$$

If  $\beta$  is approximated by:

$$\beta \cong -\frac{1}{\rho} \left( \frac{\rho_\infty - \rho}{T_\infty - T} \right)$$

then

$$\rho_\infty - \rho \cong \beta \rho (T - T_\infty)$$

(4.5)

and Eq. (4.4) becomes:

$$u \frac{\partial u}{\partial x} + v \frac{\partial u}{\partial y} = \beta g (T - T_\infty) + \gamma \frac{\partial^2 u}{\partial y^2} \quad (4.6)$$

where it is now apparent how the buoyancy force is related to the temperature difference.

For a vertical flat plate, the energy equation reduces to,

$$u \frac{\partial T}{\partial x} + v \frac{\partial T}{\partial y} = \alpha \frac{\partial^2 T}{\partial y^2} \quad (4.7)$$

where,

$$\alpha = \frac{k}{\rho C_p}$$

The set of governing boundary-layer equations describing the heat-transfer process by natural convection from a vertical flat plate may then be expressed as:

$$\frac{\partial(\rho u)}{\partial x} + \frac{\partial(\rho v)}{\partial y} = 0 \quad (\text{Continuity}) \quad (4.8)$$

$$u \frac{\partial u}{\partial x} + v \frac{\partial u}{\partial y} = \beta g (T - T_\infty) + \gamma \frac{\partial^2 u}{\partial y^2} \quad (\text{Momentum}) \quad (4.6)$$

$$u \frac{\partial T}{\partial x} + v \frac{\partial T}{\partial y} = \alpha \frac{\partial^2 T}{\partial y^2} \quad (\text{Energy}) \quad (4.7)$$

Equation (4.8) can be simplified for incompressible fluids, to:

$$\frac{\partial u}{\partial x} + \frac{\partial v}{\partial y} = 0 \quad (4.8a)$$

Based on the highest order of the dependent variables ( $u$ ,  $v$  and  $T$ ), the number of boundary conditions are: two conditions for  $u$  in  $y$  and one in  $x$ ; one condition for  $v$  in  $y$ ; and two conditions for  $T$  in  $y$  and one in  $x$ . These are:

$$\text{For } y=0, \forall x > 0: \quad u = 0, v = 0, \text{ and } T = T_w \quad (4.9)$$

$$\text{For } y = \infty, \forall x > 0: \quad u = 0, \text{ and } T = T_\infty \quad (4.10)$$

$$\text{For } x = 0, \forall y > 0: \quad u = 0, \text{ and } T = T_\infty \quad (4.11)$$

Since the momentum equation contains  $T$  and the energy equation contains  $u$  and  $v$ , Eqs. (4.6) and (4.7) are coupled and their solution must be obtained simultaneously.

### 4.3 Heat-Transfer Coefficient

The solution of the boundary-layer equations for any convection heat-transfer problem gives the velocity and temperature distributions. This is true for any type of solution (analytical or numerical) and for any type of convection (forced or natural). Once the solution is obtained, the heat-transfer coefficient is obtained by realizing that as we approach the solid surface, the velocity vector is tangent to the surface and the heat-flux vector is normal to the surface, thus the heat transfer is by conduction at the limit as the distance from the wall approaches zero. Therefore, for the problem described in the previous section:

$$-k \left( \frac{\partial T}{\partial y} \right)_{y \rightarrow 0} = h_x (T_w - T_\infty) \quad (4.12)$$

hence, the local, heat-transfer coefficient,  $h_x$  is given by:

$$h_x = -\frac{k}{(T_w - T_\infty)} \left( \frac{\partial T}{\partial y} \right)_{y \rightarrow 0} \quad (4.13)$$

Note the derivative in Eq. (4.13) is a function of  $x$ , thus,  $h_x$  is a function of  $x$ . As customarily done, the average heat-transfer coefficient for a finite flat plate of vertical length  $L$  is:

$$\bar{h}_L = \frac{1}{A'} \int_{A'} h_x dA' \quad (4.14)$$

In dimensionless form, the Nusselt numbers local and average, are defined as:

$$\text{Nu}_x = \frac{h_x x}{k} \quad \text{and} \quad \overline{\text{Nu}}_L = \frac{\bar{h}_L L}{k} \quad (4.15)$$

## **CHAPTER 5**

### **NUMERICAL SOLUTION**

#### **5.1 Introduction**

Chapter 4 presents the mathematical description of the natural-convection problem on a vertical flat plate. This resulted in three equations of change, namely Eqs. (4.6), (4.7) and (4.8). This chapter describes the numerical scheme to solve these equations. This is done by finite-differences using the fully implicit scheme in the  $y$ -direction and an explicit scheme in the  $x$ -direction. Physically, the thickness of the boundary layer is much smaller than any characteristic length defined in the streamwise direction. Therefore, the changes in physical properties in the direction parallel to the plate are small compared to the corresponding changes in the direction perpendicular to the plate. Therefore, grids in the  $y$  direction should be much finer than in the  $x$  direction. The implicit method will be most suitable for this computation because it does not require any stability condition.

#### **5.2 Numerical Model**

##### **5.2.1 Method of Finite-Differences**

One way of solving the boundary layer equations is by the finite-difference method. This method has several advantages. The method can be applied to problems involving arbitrary surface thermal conditions and arbitrary free stream velocity and is easily extended to cover the effects of variable fluid properties and

dissipation effects. The errors involved in the procedure are purely numerical and their magnitude can be estimated and generally reduced to an acceptable level by reducing the numerical step size. The disadvantages of the finite-difference method, and other numerical methods, are that a considerable amount of computational effort is usually required to obtain the solution and that they do not, in general, reveal certain unifying features of the solutions, such as the fact that profiles are similar under certain conditions. The widespread availability of modern computer facilities has, however, made these disadvantages relatively unimportant.

### **5.2.2 Description of the Solution Grid**

The finite-difference technique with an under-relaxation iterative procedure has been chosen. Subscripts  $i$  and  $j$  will be used to represent nodes in the  $x$  and  $y$  directions, respectively. Figure 5.1 shows the grid used in this work for the numerical solution. The grid chosen has a constant step size in the  $y$  direction and variable step size in the  $x$  direction, making the grid finer at the beginning of the plate for a better appreciation of the formation of the boundary layer.

### **5.2.3 Boundary-Layer Equations in Dimensionless form**

For this type of problem, although not necessary, it is often convenient to write the governing equations in dimensionless form before the deriving the finite-difference approximations. The following dimensionless variables are thus defined:

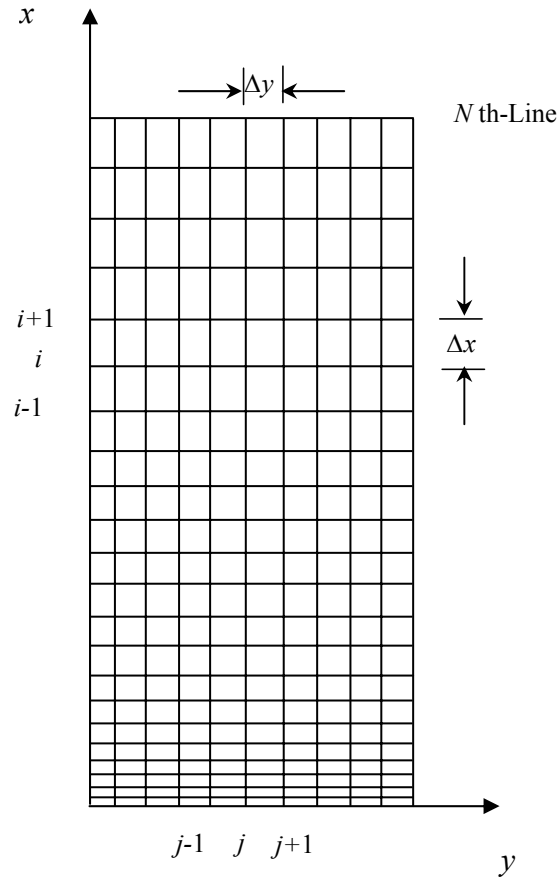


Figure 5.1. Grid used in the numerical solution.

$$\begin{aligned}
 X &= \frac{x}{LG^\circ} & Y &= \frac{y}{W} & \theta &= \frac{T - T_\infty}{T_w - T_\infty} \\
 U &= \left( \frac{uW}{\gamma} \right) \left( \frac{W}{LG^\circ} \right) & V &= \frac{vW}{\gamma} & & (5.1) \\
 G^\circ &= \frac{\beta_{ref} g (T_w - T_\infty) W^4}{\gamma^2 L} = Gr_w \frac{W}{L}
 \end{aligned}$$

where

$$\beta_{ref} = \frac{1}{T_f} \quad (5.2)$$

and

$$T_f = \frac{1}{2}(T_w + T_\infty) \quad (5.3)$$

In terms of these variables, Eqs. (4.8), (4.6), and (4.7) become, respectively:

$$\frac{\partial U}{\partial X} + \frac{\partial V}{\partial Y} = 0 \quad (5.4)$$

$$U \frac{\partial U}{\partial X} + V \frac{\partial U}{\partial Y} = \theta \beta^* + \frac{\partial^2 U}{\partial Y^2} \quad (5.5)$$

$$U \frac{\partial \theta}{\partial X} + V \frac{\partial \theta}{\partial Y} = \frac{1}{Pr} \frac{\partial^2 \theta}{\partial Y^2} \quad (5.6)$$

where

$$\beta^* = \frac{\beta}{\beta_{ref}} \quad (5.7)$$

and

$$Pr = \frac{\gamma}{\alpha}$$

When the wall temperature is uniform and the ambient fluid is stagnant, the boundary conditions given by Eqs. (4.9), (4.10), and (4.11) apply and become:

$$\begin{aligned} Y = 0: \quad U = V = 0, \theta = 1 \\ Y \rightarrow \infty: \quad U \rightarrow 0, \theta \rightarrow 0 \\ X = 0: \quad U = 0, \theta = 0 \end{aligned} \quad (5.8)$$

### 5.2.4 Finite-Difference Equations

To express the set of dimensionless partial differential equations in finite-difference form, the grid system shown in the Fig. 5.1 is used, with  $i$ -lines running in the  $Y$ -direction normal to the surface and  $j$ -lines running in the  $X$ -direction parallel to the surface. For simplicity, uniform grid spacing,  $\Delta Y$  in the  $Y$ -direction is used. Fig. 5.2 shows the notation used to derive the finite-difference equations. The equations of motion, of energy, and continuity are now discretized based on such notation.

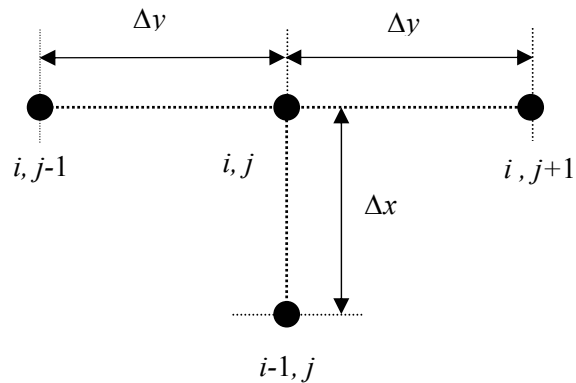


Figure 5.2. Grid points used to derive the finite-difference equations.

#### *Equation of motion*

To obtain the first finite-difference approximation for  $\partial U / \partial Y$  at the point  $(i, j)$ , a central-difference formula is used:

$$\left. \frac{\partial U}{\partial Y} \right|_{i,j} \cong \frac{U_{i,j+1} - U_{i,j-1}}{2\Delta Y} \quad (5.9)$$

The central-difference approximation to the second order derivative is given by,

$$\left. \frac{\partial^2 U}{\partial Y^2} \right|_{i,j} \cong \frac{U_{i,j+1} - 2U_{i,j} + U_{i,j-1}}{\Delta Y^2} \quad (5.10)$$

The backward-difference approximation in the  $X$ -direction is:

$$\left. \frac{\partial U}{\partial X} \right|_{i,j} \cong \frac{U_{i,j} - U_{i-1,j}}{\Delta X} \quad (5.11)$$

and

$$\left( U \frac{\partial U}{\partial X} \right) \Big|_{i,j} \cong U_{i-1,j} \left( \frac{U_{i,j} - U_{i-1,j}}{\Delta X} \right) \quad (5.12)$$

$$\left( V \frac{\partial U}{\partial Y} \right) \Big|_{i,j} \cong V_{i-1,j} \left( \frac{U_{i,j+1} - U_{i,j-1}}{2\Delta Y} \right) \quad (5.13)$$

Substituting Eqs. (5.10), (5.12), (5.13) in the momentum equation gives:

$$\left( -\frac{V_{i-1,j}}{2\Delta Y} - \frac{1}{\Delta Y^2} \right) U_{i,j-1} + \left( \frac{U_{i-1,j}}{\Delta X} + \frac{2}{\Delta Y^2} \right) U_{i,j} + \left( \frac{V_{i-1,j}}{2\Delta Y} - \frac{1}{\Delta Y^2} \right) U_{i,j+1} = \theta_{i-1,j} \beta^* + \frac{U_{i-1,j}^2}{\Delta X} \quad (5.14)$$

For each value of  $i$ , i.e., for each horizontal line in Fig. 5.1, the unknown variables are  $U_{i,j-1}$ ,  $U_{i,j}$ ,  $U_{i,j+1}$ . Therefore, Eq. (5.14) can be written in the following form:

$$C_j U_{i,j-1} + D_j U_{i,j} + E_j U_{i,j+1} = F_j \quad (5.15)$$

where the coefficients are given by:

$$C_j = \left( -\frac{V_{i-1,j}}{2\Delta Y} \right) - \left( \frac{1}{\Delta Y^2} \right) \quad (5.16)$$

$$D_j = \left( \frac{U_{i-1,j}}{\Delta X} \right) + \left( \frac{2}{\Delta Y^2} \right) \quad (5.17)$$

$$E_j = \left( \frac{V_{i-1,j}}{2\Delta Y} \right) - \left( \frac{1}{\Delta Y^2} \right) \quad (5.18)$$

$$F_j = \theta_{i-1,j} \beta^* + \left( \frac{U_{i-1,j}^2}{\Delta X} \right) \quad (5.19)$$

Note that the application of Eq. (5.15) along the  $i$ -th line in Fig. 5.1 to each of the points  $j = 2, 3, 4, \dots, N-1$ , gives a set of  $N-2$  equations and  $N-2$  unknown values of  $U$ , i.e.,  $U_2, U_3, U_4, \dots, U_{N-2}, U_{N-1}$ . This set of equations has the following form (note that  $U_{i,1}$  and  $U_{i,N}$  are zero):

$$C_2 U_{i,1} + D_2 U_{i,2} + E_2 U_{i,3} = F_2$$

$$C_3 U_{i,2} + D_3 U_{i,3} + E_3 U_{i,4} = F_3$$

$$\vdots$$

$$C_{N-1} U_{i,N-2} + D_{N-1} U_{i,N-1} + E_{N-1} U_{i,N} = F_{N-1}$$

The set of equations can thus be written in matrix form as:

$$\begin{bmatrix} D_2 & E_2 & 0 & 0 & \cdots & 0 & 0 & 0 \\ C_3 & D_3 & E_3 & 0 & \cdots & 0 & 0 & 0 \\ 0 & C_4 & D_4 & E_4 & \cdots & 0 & 0 & 0 \\ \vdots & \vdots & \vdots & \vdots & & \vdots & \vdots & \vdots \\ 0 & 0 & 0 & 0 & \cdots & C_{N-2} & D_{N-2} & E_{N-2} \\ 0 & 0 & 0 & 0 & \cdots & 0 & C_{N-1} & D_{N-1} \end{bmatrix} \begin{bmatrix} U_{i,2} \\ U_{i,3} \\ U_{i,4} \\ \vdots \\ U_{i,N-2} \\ U_{i,N-1} \end{bmatrix} = \begin{bmatrix} F_2 \\ F_3 \\ F_4 \\ \vdots \\ F_{N-2} \\ F_{N-1} \end{bmatrix}$$

or:

$$Q_U U_{i,j} = R_U \quad (5.20)$$

where  $Q_U$  is a tridiagonal matrix.

### Energy equation

Now consider the finite-difference approximations of the energy equation:

$$\left( U \frac{\partial \theta}{\partial X} \right) \Big|_{i,j} \cong U_{i-1,j} \left( \frac{\theta_{i,j} - \theta_{i-1,j}}{\Delta X} \right) \quad (5.21)$$

$$\left( V \frac{\partial \theta}{\partial Y} \right) \Big|_{i,j} \cong V_{i-1,j} \left( \frac{\theta_{i,j+1} - \theta_{i,j-1}}{2\Delta Y} \right) \quad (5.22)$$

$$\frac{\partial^2 \theta}{\partial Y^2} \Big|_{i,j} \cong \frac{\theta_{i,j+1} - 2\theta_{i,j} + \theta_{i,j-1}}{\Delta Y^2} \quad (5.23)$$

Replacing Eqs. (5.21), (5.22) and (5.23) into the energy equation and rearranging yields:

$$\left( -\frac{V_{i-1,j}}{2\Delta Y} - \frac{1}{\text{Pr} \Delta Y^2} \right) \theta_{i,j-1} + \left( \frac{U_{i-1,j}}{\Delta X} + \frac{2}{\text{Pr} \Delta Y^2} \right) \theta_{i,j} + \left( \frac{V_{i-1,j}}{2\Delta Y} - \frac{1}{\text{Pr} \Delta Y^2} \right) \theta_{i,j+1} = \frac{U_{i-1,j} \theta_{i-1,j}}{\Delta X}$$

This equation has the following form

$$G_j \theta_{i,j-1} + H_j \theta_{i,j} + S_j \theta_{i,j+1} = J_j \quad (5.24)$$

where the coefficients in this equation are given by:

$$G_j = \left( -\frac{V_{i-1,j}}{2\Delta Y} \right) - \left( \frac{1}{\text{Pr}\Delta Y^2} \right) \quad (5.25)$$

$$H_j = \left( \frac{U_{i-1,j}}{\Delta X} \right) + \left( \frac{2}{\text{Pr}\Delta Y^2} \right) \quad (5.26)$$

$$S_j = \left( \frac{V_{i-1,j}}{2\Delta Y} \right) - \left( \frac{1}{\text{Pr}\Delta Y^2} \right) \quad (5.27)$$

$$J_j = \frac{U_{i-1,j}\theta_{i-1,j}}{\Delta X} \quad (5.28)$$

The application of Eq. (5.24) to each internal point on the  $i$ -th line, e.g.,  $j = 2, 3, 4, \dots, N-1$ , gives again a set of  $N-2$  equations in the  $N-2$  unknown values of  $\theta$  (note that  $\theta_{i,1} = 1$  and  $\theta_{i,N} = 0$ ). This set of equations has the following form:

$$G_2 \theta_{i,1} + H_2 \theta_{i,2} + S_2 \theta_{i,3} = J_2$$

$$G_3 \theta_{i,2} + H_3 \theta_{i,3} + S_3 \theta_{i,4} = J_3$$

$$\vdots$$

$$G_{N-1} \theta_{i,N-2} + H_{N-1} \theta_{i,N-1} + S_{N-1} \theta_{i,N} = J_{N-1}$$

This set of equations is similar to that derived for the momentum equation, and can be expressed in matrix form as:

$$\begin{bmatrix} H_2 & S_2 & 0 & 0 & \cdots & 0 & 0 & 0 \\ G_3 & H_3 & S_3 & 0 & \cdots & 0 & 0 & 0 \\ 0 & G_4 & H_4 & S_4 & \cdots & 0 & 0 & 0 \\ \vdots & \vdots & \vdots & \vdots & & \vdots & \vdots & \vdots \\ 0 & 0 & 0 & 0 & \cdots & G_{N-2} & H_{N-2} & S_{N-2} \\ 0 & 0 & 0 & 0 & \cdots & 0 & G_{N-1} & H_{N-1} \end{bmatrix} \begin{bmatrix} \theta_{i,2} \\ \theta_{i,3} \\ \theta_{i,4} \\ \vdots \\ \theta_{i,N-2} \\ \theta_{i,N-1} \end{bmatrix} = \begin{bmatrix} J_2 - G_2 \\ J_3 \\ J_4 \\ \vdots \\ J_{N-2} \\ J_{N-1} \end{bmatrix}$$

or:

$$Q_T \theta_{i,j} = R_T$$

$$(5.29)$$

where  $Q_T$  is again a tridiagonal matrix. Thus, the same form of equation is obtained for the energy and the momentum equations.

### *Continuity equation*

There are several ways to express the continuity equation in a finite-difference form. Fig. 5.3 shows the notation used to describe the way chosen to discretize the continuity equation. The derivatives are discretized at the midpoint (not a nodal point) denoted by  $(i, j - 1/2)$  therein. This midpoint lies on the  $i$ -th line, halfway between the nodes  $(j - 1)$  and  $j$ . Applying the central-difference approximation in the  $Y$ -direction:

$$\left. \frac{\partial V}{\partial Y} \right|_{i,j-1/2} \cong \frac{V_{i,j} - V_{i,j-1}}{\Delta Y} \quad (5.30)$$

It is now assumed that the  $X$ -derivative at the point  $(i, j - 1/2)$  is equal to the average of the  $X$ -derivative at the points  $(i, j)$  and  $(i, j - 1)$ . Therefore:

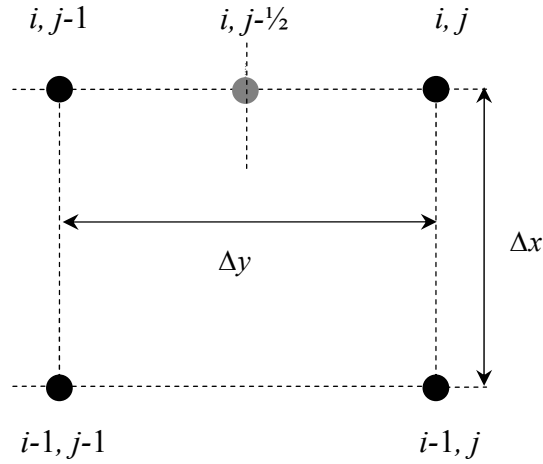


Figure 5.3. Nodal points used to discretize of the continuity equation.

$$\left. \frac{\partial U}{\partial X} \right|_{i,j-1/2} \cong \frac{1}{2} \left[ \left. \frac{\partial U}{\partial X} \right|_{i,j} + \left. \frac{\partial U}{\partial X} \right|_{i,j-1} \right] \quad (5.31)$$

Substituting Eqs. (5.30) and (5.31) into:

$$\frac{\partial V}{\partial Y} = -\frac{\partial U}{\partial X} \quad (5.32)$$

the following finite-difference approximation for the continuity equation is obtained:

$$\frac{V_{i,j} - V_{i,j-1}}{\Delta Y} = -\frac{1}{2} \left( \frac{U_{i,j} - U_{i-1,j}}{\Delta X} + \frac{U_{i,j-1} - U_{i-1,j-1}}{\Delta X} \right) \quad (5.33)$$

from which the following expression for  $V_{i,j}$  obtained is:

$$V_{i,j} = V_{i,j-1} - \left( \frac{\Delta Y}{2\Delta X} \right) (U_{i,j} - U_{i-1,j} + U_{i,j-1} - U_{i-1,j-1}) \quad (5.34)$$

In summary, this section has presented the derivation of the three main discretized equations. These are Eqs. (5.20), (5.29), and (5.34).

### 5.2.5 Thomas Algorithm to Solve a Tridiagonal System of Equations

When written for each value of  $X$  in the grid (or each value of  $i$ ), the discretized equations obtained in the previous section generate two sets of simultaneous, linear, algebraic equations whose matrices of coefficients are tridiagonal. This type of problem may be solved by a Gauss elimination procedure or, more efficiently, by the Thomas algorithm, a variation of Gauss elimination.

Implicit formulas of the type described above have been found to be unconditionally stable. Thomas algorithm is essentially the result of applying Gauss elimination to the tridiagonal system of equations. In this method, the lower-diagonal is first eliminated. The details are shown below for the momentum equation first, and then for the energy equation.

#### *Momentum Equation*

Applying Gauss elimination to Eq. (5.15) to eliminate the lower-diagonal term (the  $C_j$ 's) results in an upper bidiagonal form of equations given by

$$\begin{array}{rcl}
 U_{i,2} + \frac{E_2}{\alpha'_2} U_{i,3} & & = \Psi_2 \\
 U_{i,3} + \frac{E_3}{\alpha'_3} U_{i,4} & & = \Psi_3 \\
 & \vdots & \\
 U_{i,N-2} + \frac{E_{N-2}}{\alpha'_{N-2}} U_{i,N-1} & = & \Psi_{N-2} \\
 U_{i,N-1} & = & \Psi_{N-1}
 \end{array}$$

The last equation, contains only one unknown, namely,  $U_{i,N-1}$ , hence

$$U_{i,N-1} = \Psi_{N-1} \quad (5.35)$$

The solution of the remaining unknown is obtained by working *upward* in the above system. First,  $U_{i,N-1}$  is obtained from Eq. (5.35), then  $U_{i,N-2}$  is found from the penultimate equation as

$$U_{i,N-2} = \Psi_{N-2} - \frac{E_{N-2}}{\alpha'_{N-2}} U_{i,N-1} \quad (5.36)$$

and so on. The following general recursion formula is thus obtained:

$$U_{i,j} = \Psi_j - \frac{E_j}{\alpha'_j} U_{i,j+1} \quad \text{for } j = N-2, N-3, \dots, 2 \quad (5.37)$$

Decreasing the values of  $j$  from  $j = N-2$  down to  $j = 2$  lead to an explicit solution provided that the  $\alpha'$ 's are known. The computation of  $\alpha'$ 's is done forward from  $j = 2$  up to  $j = N-1$ . For  $j = 2$ :

$$\alpha'_2 = D_2 \quad (5.38)$$

and for the rest of the equations:

$$\alpha'_j = D_j - C_j \frac{E_{j-1}}{\alpha'_{j-1}} \quad \text{for } j = 3, 4, \dots, N-1 \quad (5.39)$$

Similarly, the computation of the  $\psi$ 's starts with  $j = 2$ :

$$\Psi_2 = \frac{F_2}{\alpha'_2} \quad (5.40)$$

and then for the rest of the  $\psi_j$ 's :

$$\psi_j = \frac{F_j - C_j \psi_{j-1}}{\alpha'_j} \quad \text{for } j=3, 4, \dots, N-1 \quad (5.41)$$

### *Energy Equation*

The solution of the energy equations is quite similar to the solution of the momentum equation. First, Gauss elimination is applied to Eq. (5.24) to eliminate the lower-diagonal term (the  $G_j$ 's). The following upper bidiagonal form of equations results:

$$\begin{aligned} \theta_{i,2} + \frac{S_2}{\phi_2} \theta_{i,3} &= \rho'_2 \\ \theta_{i,3} + \frac{S_3}{\phi_3} \theta_{i,4} &= \rho'_3 \\ &\vdots \\ \theta_{i,N-2} + \frac{S_{N-2}}{\phi_{N-2}} \theta_{i,N-1} &= \rho'_{N-2} \\ \theta_{i,N-1} &= \rho'_{N-1} \end{aligned}$$

Again, the solution of the  $\theta_{i,j}$  starts from  $j = N - 1$ :

$$\theta_{i,N-1} = \rho'_{N-1} \quad (5.42)$$

and continues backward from  $j = N - 2$  down to  $j = 2$  applying the following equation :

$$\theta_{i,j} = \rho'_j - \frac{S_j}{\phi_j} \theta_{i,j+1} \quad \text{for } j = N - 2, N - 3, \dots, 2 \quad (5.43)$$

The  $\phi_j$ 's are calculated from  $j = 2$  :

$$H_2 = \phi_2 \quad (5.44)$$

and then for  $j = 3$  up to  $j = N - 1$ , the  $\phi_j$ 's are:

$$\phi_j = H_j - G_j \frac{S_{j-1}}{\phi_{j-1}} \quad \text{for } j = 3, 4, \dots, N-1 \quad (5.45)$$

Finally, the  $\rho_j$ 's are computed first for  $j = 2$ :

$$\rho'_2 = \frac{J_2 - G_2}{\phi_2} \quad (5.46)$$

and then on, for the rest of the  $j$ 's:

$$\rho'_j = \frac{J_j - \rho'_{j-1} G_j}{\phi_j} \quad \text{for } i = 3, 4, \dots, N-1 \quad (5.47)$$

#### *Parameters in dimensional form*

Once the dimensionless profiles are known, the dimensional variables are calculated with the following transformations:

$$u = U \frac{\gamma L G}{W^2} \quad v = \frac{V \gamma}{W} \quad T = (T_w - T_\infty)\theta + T_\infty \quad \beta^* = \frac{\beta}{\beta_{ref}} \quad (5.48)$$

#### **5.2.6 Relaxation Technique**

For the solution of the three coupled equations, an iterative procedure was used with an under-relaxation coefficient of 0.2 for a quicker convergence of the temperatures and velocities. Under-relaxation is used when the equations are non-linear; the relaxation coefficient must be between 0 and 1. This technique appears to be most appropriate when the convergence shows an oscillatory pattern and

tends to overshoot the apparent final solution. Flow diagrams of the numerical code are shown in the following section.

### 5.3 Calculation of the Heat-Transfer Coefficient

The numerical calculation of the heat-transfer coefficient, once the temperature field is obtained as described in this previous section, is based on Eq. (4.13):

$$h_x = -\frac{k}{(T_w - T_\infty)} \left( \frac{\partial T}{\partial y} \right)_{y \rightarrow 0} \quad (4.13)$$

The derivative therein is calculated numerically by taking the first row of temperature in numerical solution, i.e.,  $T(i, 2)$ . Note that  $T(i, 1) = T_w$ . Therefore:

$$\left( \frac{\partial T}{\partial y} \right)_{y \rightarrow 0} \cong \frac{T(i, 2) - T_w}{\Delta y}$$

(5.49)

Once  $h_x$  is obtained, the following dimensionless numbers are computed.

$$\text{Nu}_x = \frac{h_x x}{k} \quad \text{Ra}_x = \frac{\beta_{ref} g (T_w - T_\infty) x^3}{\gamma \alpha}$$

### 5.4 Program Description

A FORTRAN code was written to carry out the calculations described in this Chapter. The dimensionless velocity profiles ( $U$  and  $V$ ) are calculated first; then, the temperature profiles ( $\theta$ ). These sequential calculations are repeated until

reaching convergence. Then, the corresponding dimensional profiles are obtained. Appendix C contains this FORTRAN code.

Figure 5.4, which spans four pages, shows a flowchart of the algorithm of the main program. The flowchart for the subroutines that calculate the compressibility factor (ZETA), thermal expansion coefficient (CALCBETA), and Thomas algorithm (TRISOL) are shown in the Figs. 5.5, 5.6, and 5.7, respectively.

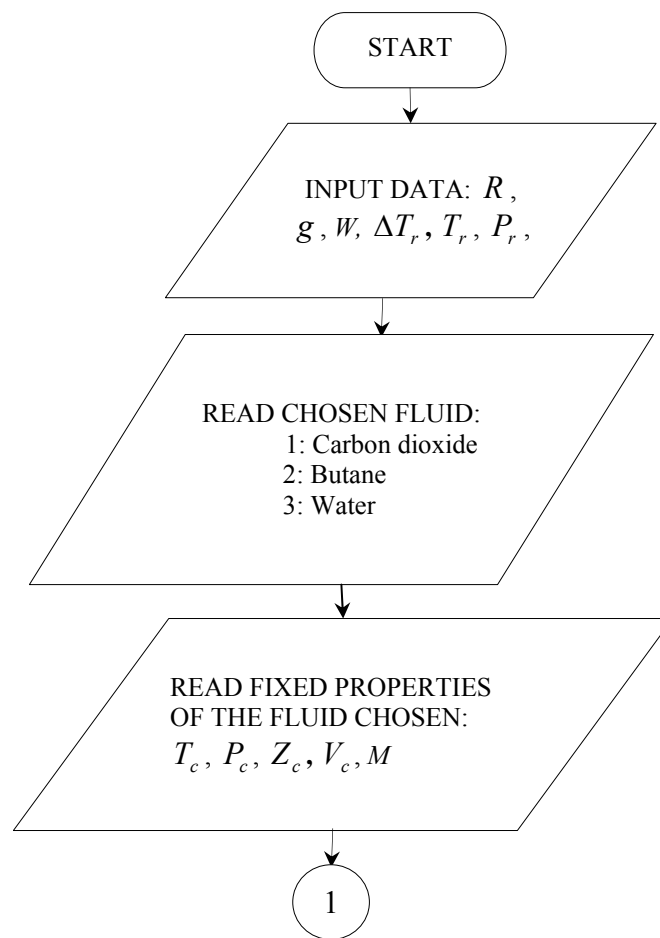


Figure 5.4. General flowchart of the program.

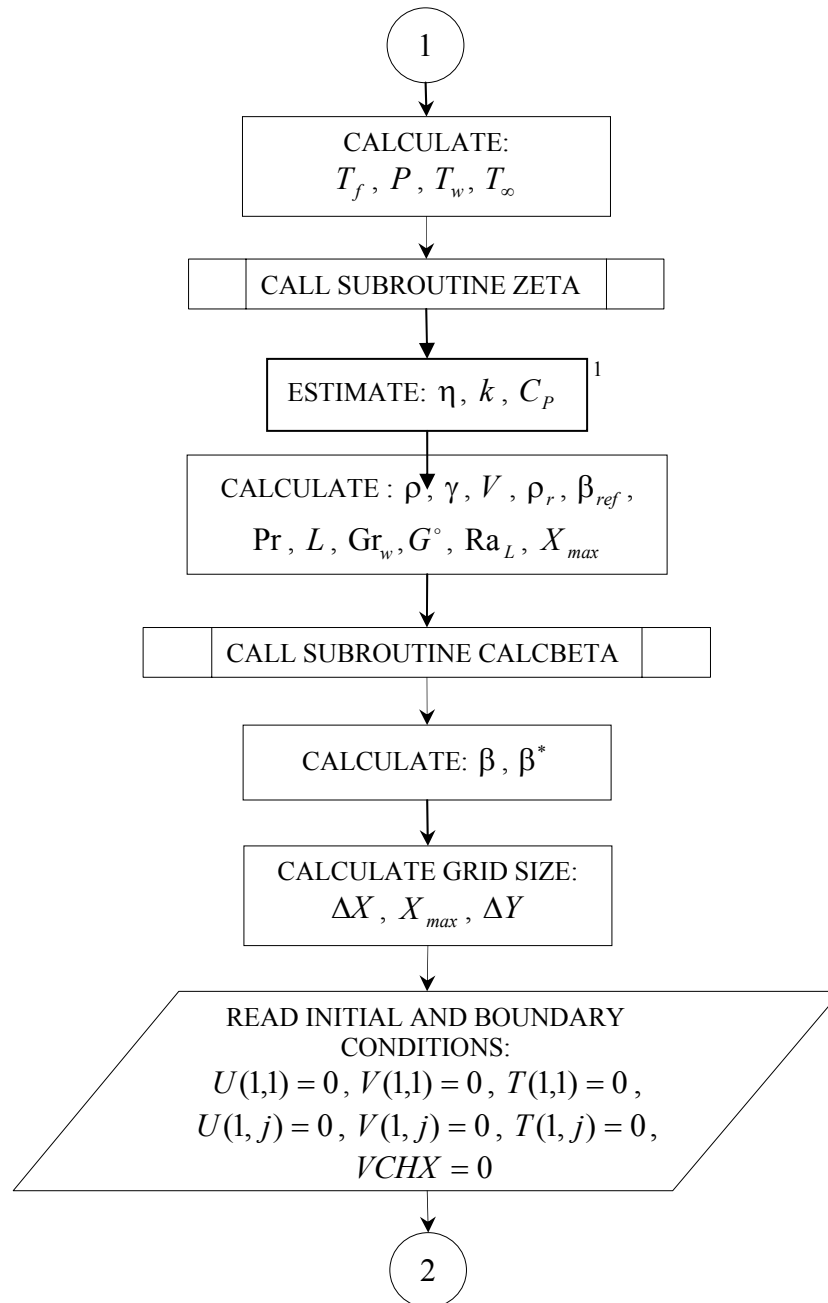


Figure 5.4. (Cont.)

<sup>1</sup> Estimation of viscosity, thermal conductivity, and heat capacity at supercritical conditions is explained in Chapter 6.

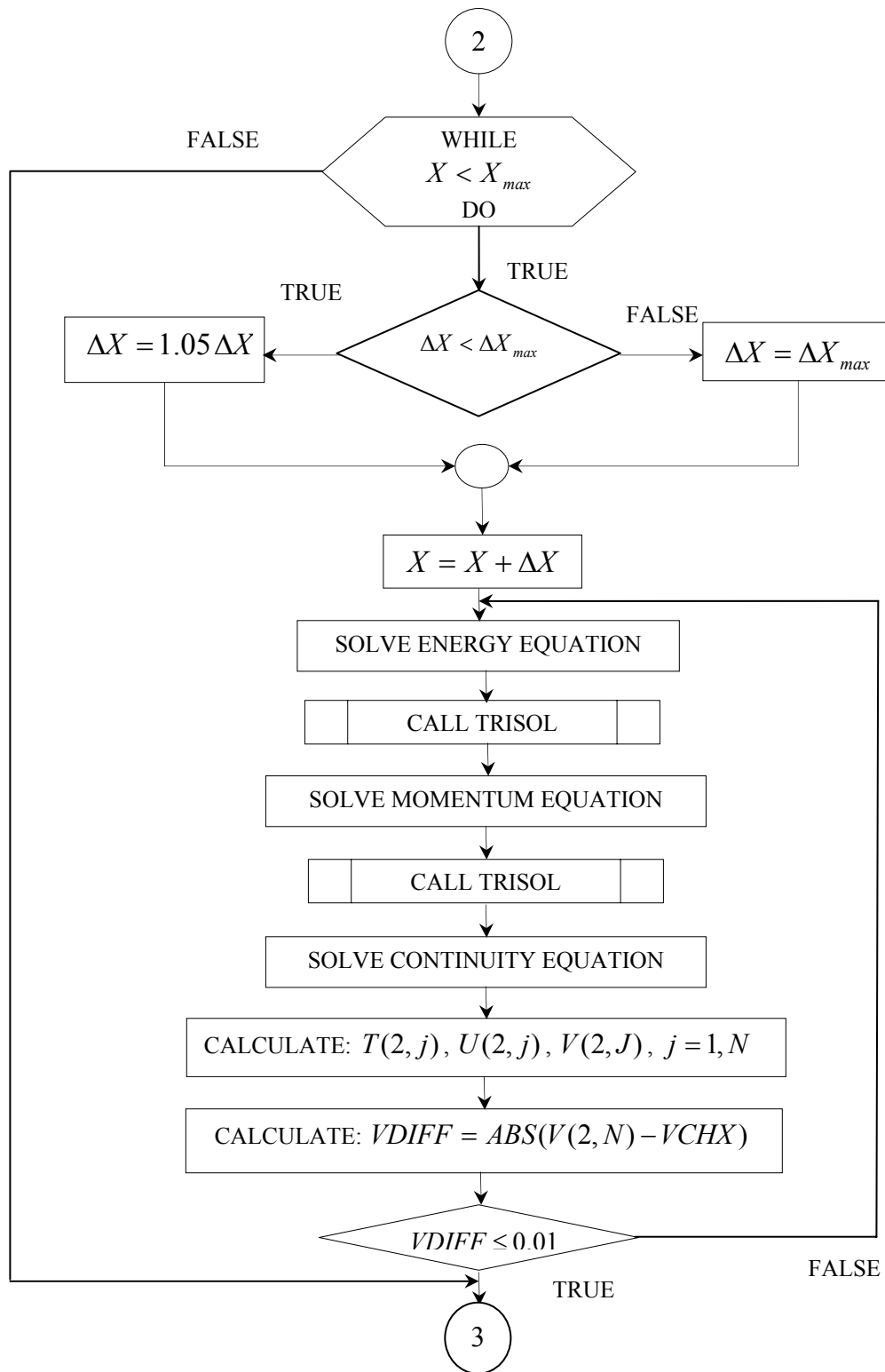


Figure 5.4. (Cont.)

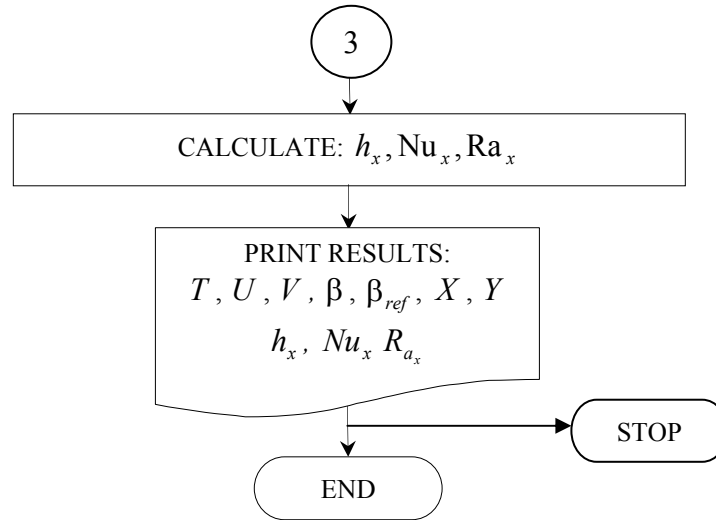


Figure 5.4. (Cont.)

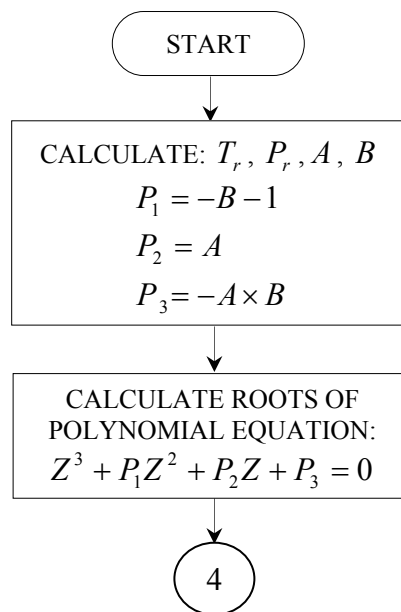


Figure 5.5. Flowchart for subroutine ZETA.

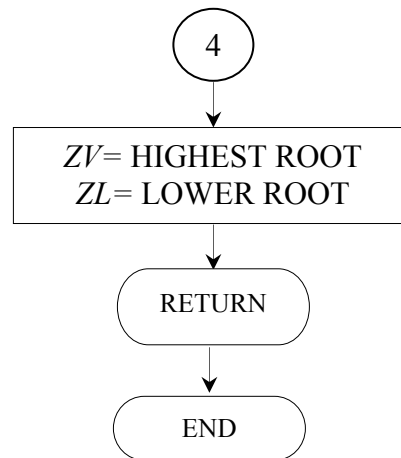


Figure 5.5. (Cont.)

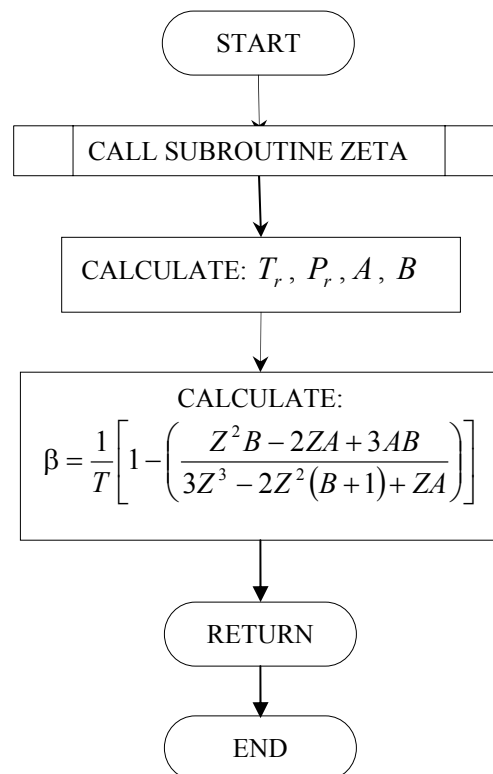


Figure 5.6. Flowchart for subroutine CALCBETA.

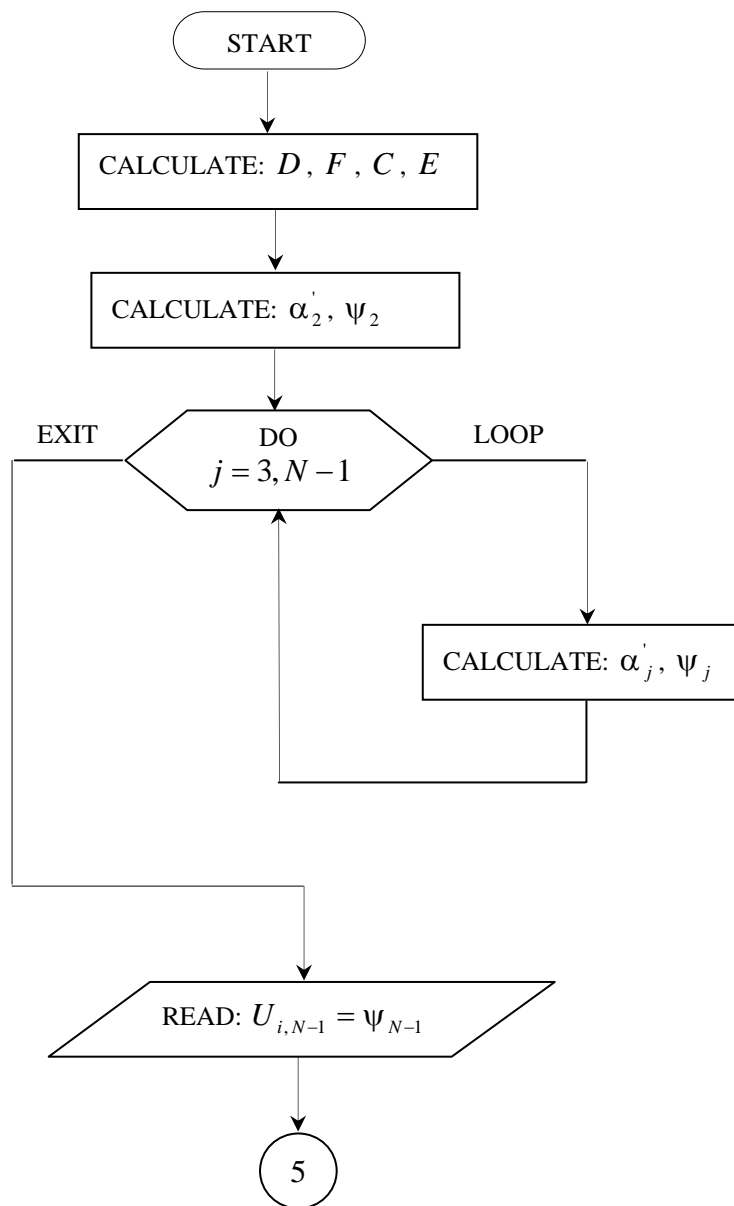


Figure 5.7. Flowchart for subroutine TRISOL.

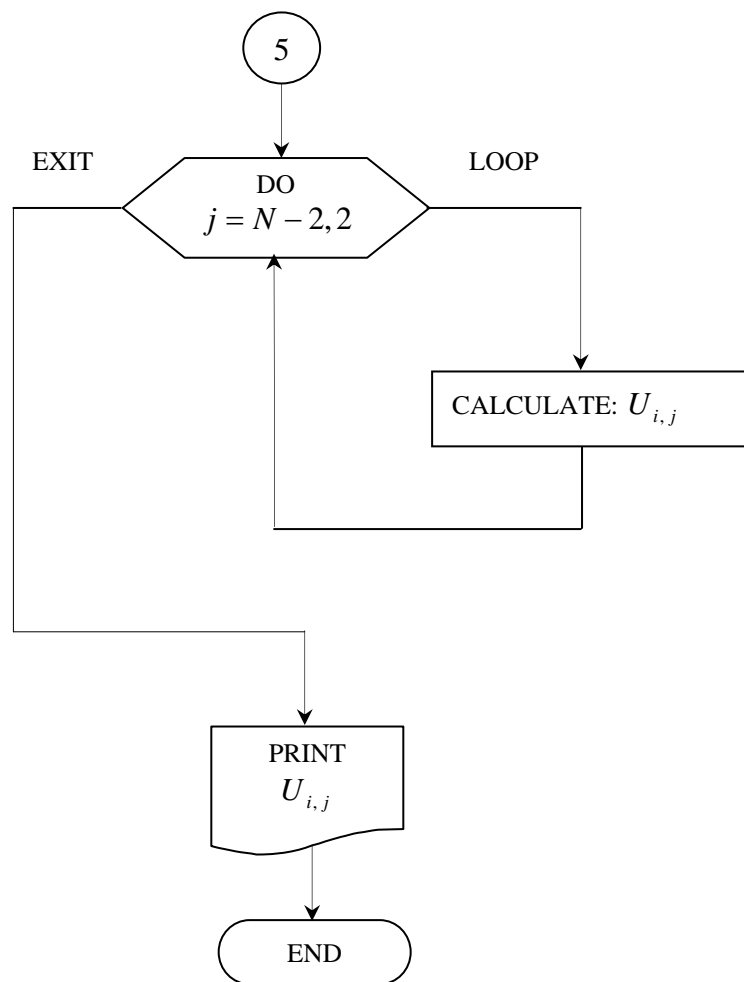


Figure 5.7. (Cont.)

## CHAPTER 6

### ESTIMATION OF FLUID PROPERTIES AND DESIGN OF RUNS

#### 6.1 Fluids Selected

Three fluids have been selected to run the simulations in this thesis. These are carbon dioxide, butane, and water. Carbon dioxide is an obvious choice given its widespread use in practical applications, as mentioned in Chapter 1, section 1.1 of this thesis. Extensive tabulation of properties are available in [2]. Light hydrocarbons constitute a group of substances that are also used in many applications, particularly in the petroleum sector. Butane has been chosen to represent this group. Detailed thermodynamic properties are tabulated in [7]. Finally, water is extensively used in a specific type of supercritical process called supercritical water oxidation (often referred to as SCWO). This and the extensive availability of properties (e.g., Keenan and Keyes, [12]) made water the third selected substance for this study. The main properties of the selected substances are shown in Table 6.1.

Table 6.1. Critical parameters of the fluids using for program running

Fluid	$P_c$ [MPa]	$T_c$ [K]	$M$ [g/mol]	$V_c$ [cm <sup>3</sup> /mol]	$Z_c$ [-]
carbon dioxide	7.380	304.20	44.010	94.07	0.274
butane	3.796	425.16	58.123	255.00	0.274
water	22.090	647.30	18.015	55.95	0.229

## 6.2 Design of Runs

The design of the simulations runs was based on the theory of design of experiments (sometimes abbreviated as DoE). In DoE terminology, the design selected is a  $3^n$  factorial for each substance [15]. For two variables and three levels, the number of runs for each substance is  $3^2$  or 9. The variables chosen are reduced pressure and reduced temperature, defined as:

$$P_r = \frac{P}{P_c} \quad (6.1)$$

$$T_r = \frac{T}{T_c} \quad (6.2)$$

The levels (values) chosen for  $P_r$  and  $T_r$  are: 1, 1.05 and 1.10. Fig. 6.1 shows schematically the factorial simulation design selected.

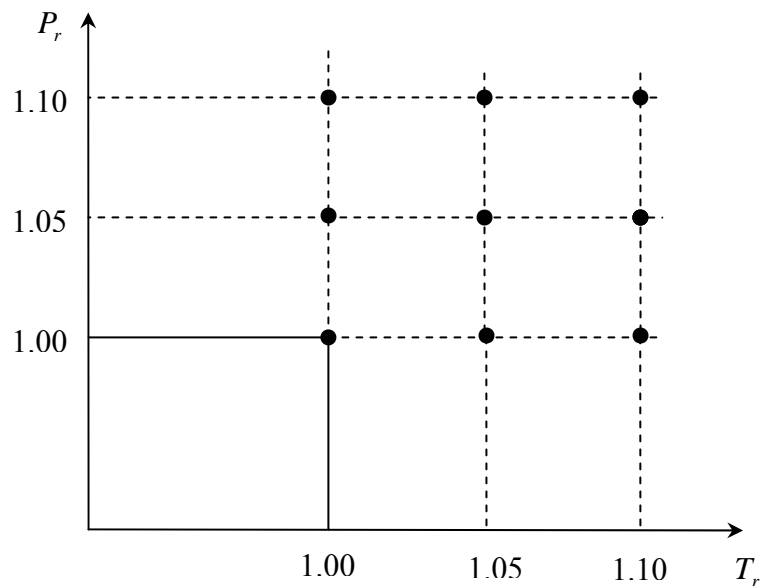


Figure 6.1. Points in the supercritical region for the simulation analysis.

If the effect of  $T_r$  and  $P_r$  is to be investigated, only 5 runs are required. Therefore, the corner points in Fig. 6.1 were not used in this work. Also, calculations at far-from-critical conditions ( $P_r = 0.2$ , and  $T_r = 0.2$ ) and by an empirical correlation proposed by Churchill and Chu [6] were done for comparison purposes.

Besides the basic properties presented in Table 6.1, the simulations require other transport and thermodynamic properties not readily available at supercritical conditions. These are viscosity, thermal conductivity, and heat capacity. The following sections describe the way these properties were estimated.

### 6.3 Viscosity Estimation

The procedure used to estimate the viscosity of the fluids at supercritical conditions has been taken from Poling et al. [22]. This method is recommended for dense fluids at super- or near-critical conditions. Figure 9.6 of reference [22] presents the product  $\eta\xi$  as a function of  $T_r$ , where  $\eta$  is the viscosity in [Pa·s], and  $\xi$  is defined as:

$$\xi = 0.176 \left( \frac{T_c}{M^3 P_c^4} \right)^{1/6} \quad (6.3)$$

where  $T_c$  is in [K],  $P_c$  in [bar], and  $M$  in [g/mol].

Note that  $\xi$  is a unique property of each fluid that does not depend on  $T$  or  $P$ . The values for the substances selected in this work are presented in Table 6.2.

The viscosity values calculated for these substances at the nine conditions of the 3<sup>n</sup> factorial design are presented in Table 6.3.

Table 6.2. Inverse viscosity

Fluid	$\xi \times 10^3$ [ $\mu\text{P}$ ] <sup>-1</sup>
carbon dioxide	3.9124
butane	5.6045
water	3.3399

Table 6.3. Dynamic viscosity for the fluids near the critical point

$T_r$	$P_r$	$\eta \xi$	$\eta$ [ $\mu\text{P}$ ]		
			carbon dioxide	butane	water
1.00	1.00	0.90	230.0383	160.5842	269.4657
	1.05	0.98	250.4861	174.8583	293.4182
	1.10	1.10	281.1579	196.2695	329.3469
1.05	1.00	0.85	217.2584	151.6628	254.4953
	1.05	0.88	224.9263	157.0156	263.4775
	1.10	0.92	235.1502	164.1527	275.4538
1.10	1.00	0.83	212.1464	148.0943	248.5072
	1.05	0.85	217.2584	151.6628	254.4953
	1.10	0.87	222.3703	155.2314	260.4835

#### 6.4 Thermal conductivity

The thermal conductivity of fluids varies considerably from dilute gas to compressed liquid, or from vapor to supercritical fluid. It is, therefore impossible to predict the behavior of the thermal conductivity, especially of supercritical fluids, without a detailed experimental and theoretical study. Knowledge of the thermal conductivity is also very important in the development of molecular theories of fluids and fluid mixtures. The method used in this work is the one proposed by Stiel and Thodos [26]. They used dimensional analysis to obtain a correlation between  $k - k^0$ ,  $Z_c$ ,  $\Gamma$ , and  $\rho_r$ . Then, they established the following approximate analytical expressions:

$$k = \begin{cases} k^0 + \frac{1.22 \times 10^{-2} [\exp(0.535 \rho_r) - 1]}{\Gamma Z_c^5} & \rho_r < 0.5 \\ k^0 + \frac{1.14 \times 10^{-2} [\exp(0.67 \rho_r) - 1.069]}{\Gamma Z_c^5} & 0.5 < \rho_r < 2.0 \\ k^0 + \frac{2.60 \times 10^{-3} [\exp(1.155 \rho_r) + 2.016]}{\Gamma Z_c^5} & 2.0 < \rho_r < 2.8 \end{cases} \quad (6.4)$$

where  $k^0$  is the ideal-gas or low-pressure limit of the thermal conductivity,  $\rho_r$  is the reduced density, calculated in this work as:

$$\rho_r = \frac{3}{8} \frac{PT_c}{ZT_f P_c} \quad (6.5)$$

and  $\Gamma$  is a parameter defined by:

$$\Gamma = 210 \left( \frac{T_c M^3}{P_c^4} \right)^{1/6} \quad (6.6)$$

where  $k^0$  is in [W/m·K],  $T_c$  in [K],  $P_c$  in [bar], and  $M$  in [g/mol].

Table 6.4 shows the thermal conductivity ( $k^0$ ) obtained from tables of gases at atmospheric pressure and at the temperatures corresponding to the 3<sup>n</sup> factorial design for the carbon dioxide, butane and, water. The actual values of  $k$  are calculated in the program using the Eq. (6.4).

Table 6.4. Low-pressure thermal conductivity of the gas

Fluid	$T_r$	$T$ [K]	$k^0 \times 10^3$ [W/m·K]
carbon dioxide	1.00	304.20	16.882
	1.05	319.41	18.006
	1.10	334.62	19.256
butane	1.00	425.16	30.176
	1.05	446.42	32.934
	1.10	467.68	35.691
water	1.00	647.30	46.134
	1.05	679.66	48.871
	1.10	712.03	51.615

## 6.5 Heat capacity

The heat capacities of real gases are related to the corresponding value in the ideal-gas or low-pressure state, (at the same temperature and composition) by the following definition:

$$C_p = C_p^0 + \Delta C_p \quad (6.7)$$

where  $\Delta C_p$  is the so-called residual heat capacity. (This definition can be applied to a pure gas or to a gas mixture at constant composition.) The residual heat capacity can be estimated from the Lee-Kesler [13] correlation as a function of  $T_r$  and  $P_r$ :

$$\Delta C_p \equiv C_p - C_p^0 = (\Delta C_p)^{(0)} + \omega(\Delta C_p)^{(1)}$$

or, in dimensionless form:

$$\frac{C_p - C_p^0}{R} = \left( \frac{C_p - C_p^0}{R} \right)^{(0)} + \omega \left( \frac{C_p - C_p^0}{R} \right)^{(1)} \quad (6.8)$$

$$C_p = R \left( \frac{C_p - C_p^0}{R} \right)^{(0)} + \omega R \left( \frac{C_p - C_p^0}{R} \right)^{(1)} + C_p^0 \quad (6.9)$$

The contributions  $\left( \frac{C_p - C_p^0}{R} \right)^{(0)}$  and  $\left( \frac{C_p - C_p^0}{R} \right)^{(1)}$  can be obtained from Tables 5.8

and 5.9 of Reid et al. [24], respectively. At atmospheric pressure, the isobaric, ideal-gas heat capacity is given by [24]:

$$C_p^0 = CPA + (CPB)T + (CPC)T^2 + (CPD)T^3 \quad (6.10)$$

where  $C_p^0$  is in [J/mol·K],  $T$  is in [K], and the constants  $CPA$  through  $CPD$  are given in Table 6.5.

Table 6.5. Constants to calculate the isobaric heat capacity

	$CPA$	$CPB$	$CPC$	$CPD$
carbon dioxide	19.80	734.4	$-5.602 \times 10^{-5}$	$1.715 \times 10^{-8}$
butane	9.487	0.3313	$-1.108 \times 10^{-4}$	$-2.822 \times 10^{-9}$
water	32.24	$1.924 \times 10^{-3}$	$1.055 \times 10^{-5}$	$-3.596 \times 10^{-9}$

Equation (6.9) was used to calculate the heat capacity of the three fluids selected for this study at the nine conditions of the simulations design. Unfortunately, Tables 5.8 and 5.9 of Reid et al. [24] have a few empty cells (filled with asterisks). When the value of one of those empty cells was needed, it had to be estimated using an extrapolation procedure described in Appendix B. Tables 6.6, 6.7 and 6.8 show the resulting heat capacity values for carbon dioxide, butane, and water, respectively. Note that these tables show a total of 55 possible combinations of  $P_r$  and  $T_r$ . This is much more than needed for this work, but their inclusion in the program gives it added capabilities for future work.

Table 6.6. Heat capacities for carbon dioxide

$P_r$	$C_p$ [kJ/kg·K]				
	$T_r = 1.20$	$T_r = 1.15$	$T_r = 1.10$	$T_r = 1.05$	$T_r = 1.00$
<b>0.20</b>	0.969	0.965	0.963	0.965	0.971
<b>0.40</b>	1.040	1.051	1.070	1.101	1.152
<b>0.60</b>	1.126	1.160	1.214	1.304	1.472
<b>0.80</b>	1.231	1.303	1.422	1.653	2.299
<b>1.00</b>	1.362	1.494	1.745	2.410	100000.000
<b>1.05</b>	1.399	1.550	1.855	3.125	16.667
<b>1.10</b>	1.439	1.618	1.976	4.032	10.000
<b>1.20</b>	1.524	1.757	2.291	4.791	6.536
<b>1.50</b>	1.834	2.315	3.562	4.255	3.597
<b>2.00</b>	2.348	2.961	47.619	3.279	2.434
<b>3.00</b>	2.416	2.519	#N/A	2.205	2.035

Table 6.7. Heat capacities for butane

$P_r$	$C_p$ [kJ/kg·K]				
	$T_r = 1.20$	$T_r = 1.15$	$T_r = 1.10$	$T_r = 1.05$	$T_r = 1.00$
<b>0.20</b>	4.081	4.009	3.936	3.864	3.794
<b>0.40</b>	4.133	4.071	4.013	3.962	3.923
<b>0.60</b>	4.196	4.151	4.118	4.108	4.152
<b>0.80</b>	4.274	4.255	4.269	4.362	4.744
<b>1.00</b>	4.370	4.397	4.508	4.921	100000.000
<b>1.05</b>	4.405	4.444	4.566	5.747	15.873
<b>1.10</b>	4.425	4.484	4.630	6.410	11.236
<b>1.20</b>	4.492	4.594	4.921	6.752	8.696
<b>1.50</b>	4.727	5.021	5.884	6.494	6.061
<b>2.00</b>	5.111	5.478	9.346	5.780	4.831
<b>3.00</b>	5.125	5.114	#N/A	4.739	4.543

Table 6.8. Heat capacities for water

$P_r$	$C_p$ [kJ/kg·K]				
	$T_r = 1.20$	$T_r = 1.15$	$T_r = 1.10$	$T_r = 1.05$	$T_r = 1.00$
<b>0.20</b>	2.297	2.304	2.319	2.345	2.386
<b>0.40</b>	2.489	2.538	2.611	2.720	2.890
<b>0.60</b>	2.719	2.831	3.002	3.277	3.784
<b>0.80</b>	2.996	3.207	3.554	4.219	6.098
<b>1.00</b>	3.331	3.700	4.390	6.189	100000.000
<b>1.05</b>	3.436	3.861	4.651	7.813	52.632
<b>1.10</b>	3.534	4.016	4.975	9.901	32.258
<b>1.20</b>	3.738	4.356	5.730	11.770	19.231
<b>1.50</b>	4.488	5.690	8.832	10.638	9.346
<b>2.00</b>	5.793	7.533	22.222	8.547	6.552
<b>3.00</b>	6.275	6.700	#N/A	5.917	5.456

## CHAPTER 7

### RESULTS AND DISCUSSION

#### 7.1 Thermodynamic Analysis

##### 7.1.1 Reference Values for $\beta$

Chapter 3 of this thesis presents a thermodynamic model to estimate  $\beta$  for dense gases. This model was used to calculate  $\beta$  for the three substances selected in this study. It would be desirable to compare the calculated values to experimental ones. Unfortunately, to the author's knowledge, no such data exist. Alternatively, the calculated values are compared to: (i) ideal-gas values, (ii) liquid-phase values (in the case of water) and (iii) values obtained from tabulated densities. The values obtained from tabulated, accurate densities are assumed to be accurate values of  $\beta$  therefore will be used in lieu of experimental values, and will be referred to as *reference* values in the remainder of this thesis.

For all three substances, the ideal-gas the thermal expansivity coefficient was calculated as the inverse absolute temperature. The thermal expansivity coefficient for liquid water was taken from the Appendix I of Welty et al. [27]. The reference values of  $\beta$  are calculated using the definition of  $\beta$  as a starting point.

$$\beta = -\frac{1}{\rho} \left( \frac{\partial \rho}{\partial T} \right)_p \quad (7.1)$$

Then, the partial derivative of  $\beta$  in Eq. (7.1) is substituted by its numerical approximation along the isobar corresponding to pressure  $P$  in the table:

$$\beta_i \cong -\frac{1}{\rho_i} \left( \frac{\rho_{i+1} - \rho_{i-1}}{T_{i+1} - T_{i-1}} \right)_P$$

where  $\rho_{i-1}$ ,  $\rho_i$  and  $\rho_{i+1}$  are consecutive values in the table at  $T_{i-1}$ ,  $T_i$  and  $T_{i+1}$ , respectively. The resulting  $\beta_i$  is the reference value at  $T_i$  and  $P$ .

The tabulated densities for each of three substances used in this work were obtained from references indicated in Table 7.1.

Table 7.1. Bibliography used for tabulated densities

Fluid	Reference
carbon dioxide	Angus et al. [2]
butane	Haynes and Goodwin [7], Table 21
water	Keenan et al. [11]

### 7.1.2 Results

This section presents results of  $\beta$  calculated by the thermodynamic model developed in Chapter 3, based on the van der Waals EOS, Eq. (3.17). These values are presented graphically, where they are compared to ideal-gas and reference values. In this part of the thesis, for the water the calculation were carried out a three different pressures:  $0.5P_c$ ,  $P_c$ ,  $1.5P_c$ , i.e., values of reduced pressure of 0.5, 1, and 1.5. For the carbon dioxide the pressures used were: 3.69 MPa ( $0.5P_c$ ),

7.38 MPa ( $P_c$ ), and 10 MPa. Finally, for the butane the pressures were: 1.80 MPa, 3.796 MPa ( $P_c$ ), and 5.50 MPa.

Figures (7.1), (7.2), and (7.3) represent three  $\beta$  versus  $T$  isobars for this fluid where the values calculated are compared to the reference values. It can be seen that the van der Waals equation of state, despite its simplicity, does provide an excellent representation of the data. Also interesting is the fact that  $\beta$  diverges at the critical point ( $T_r = 1$ ,  $P_r = 1$ ), and this happens regardless of the EOS used. Fig. 7.4 shows the three isobars including the calculated values. The ideal-gas  $\beta$  is included for comparison purposes.

It is well known that  $\beta$  for liquids at low (atmospheric) pressure increases with temperature, while the opposite is true for low-pressure gases. Higher-pressure isobars show a liquid-like behavior at lower (subcritical) temperatures, a gas-like behavior at higher (supercritical) temperatures, and a maximum at an intermediate temperature, close but not necessarily equal to  $T_c$ . At even higher temperatures, all isobars approach the ideal-gas behavior.

Figures (7.5), (7.6), (7.7), and (7.8) for butane and Figs. (7.9), (7.10), (7.11), and (7.12) for water show similar plots, where the qualitative observations presented above for carbon dioxide apply equally well to the others fluids.

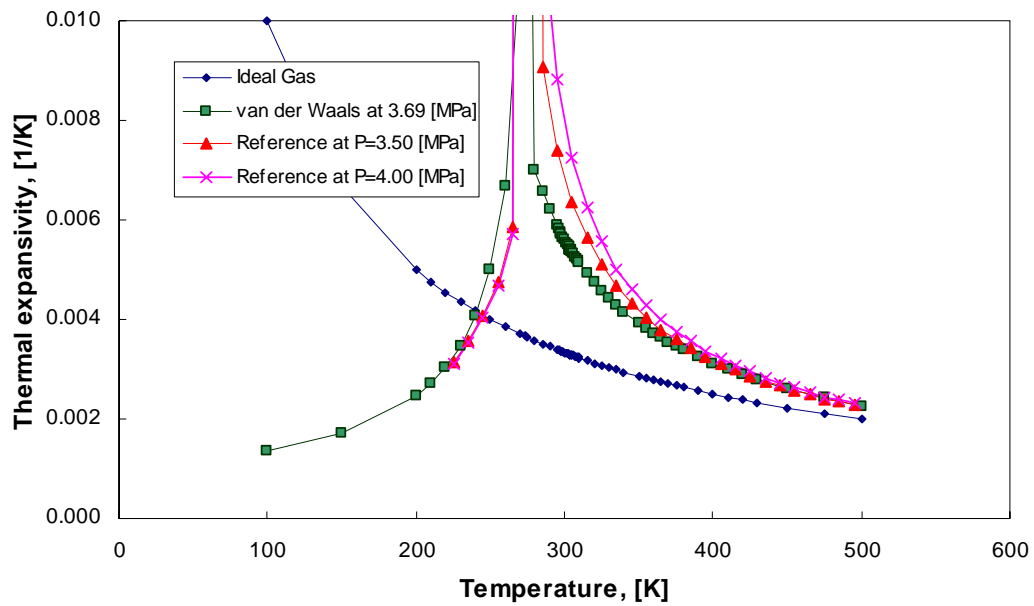


Figure 7.1. Thermal expansion coefficient of carbon dioxide at 3.69 [MPa].

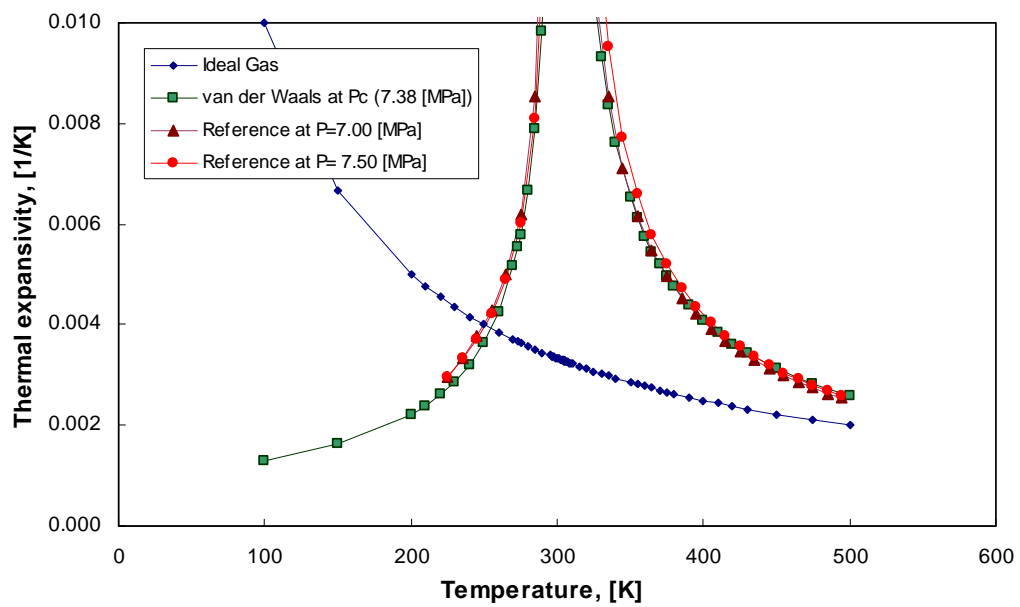


Figure 7.2. Thermal expansion coefficient of carbon dioxide at its critical pressure.

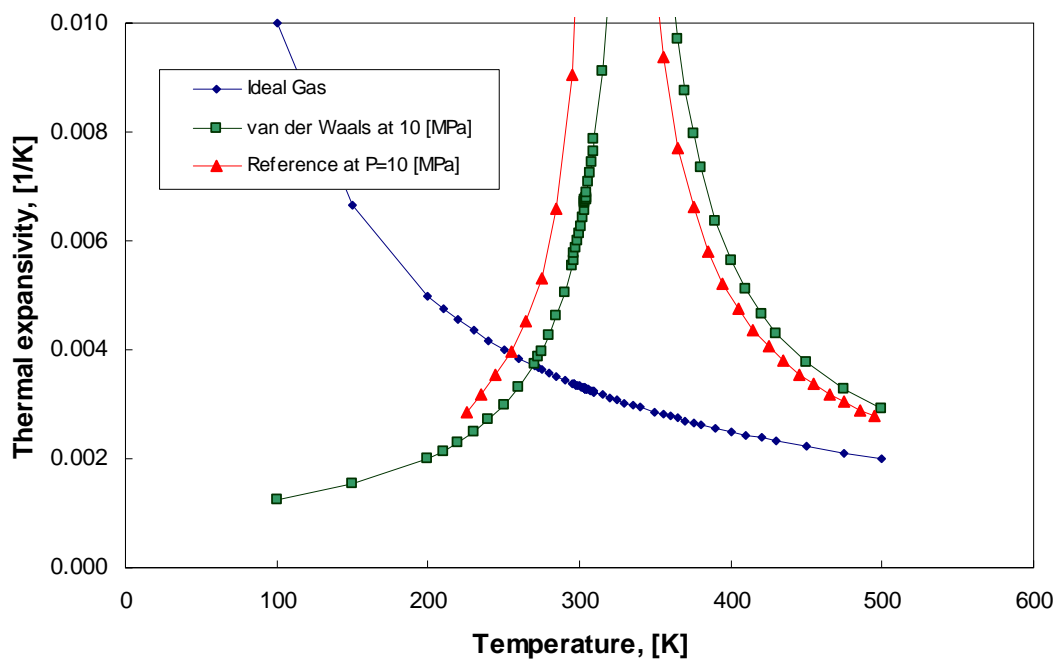


Figure 7.3. Thermal expansion coefficient of carbon dioxide at 10 [MPa].

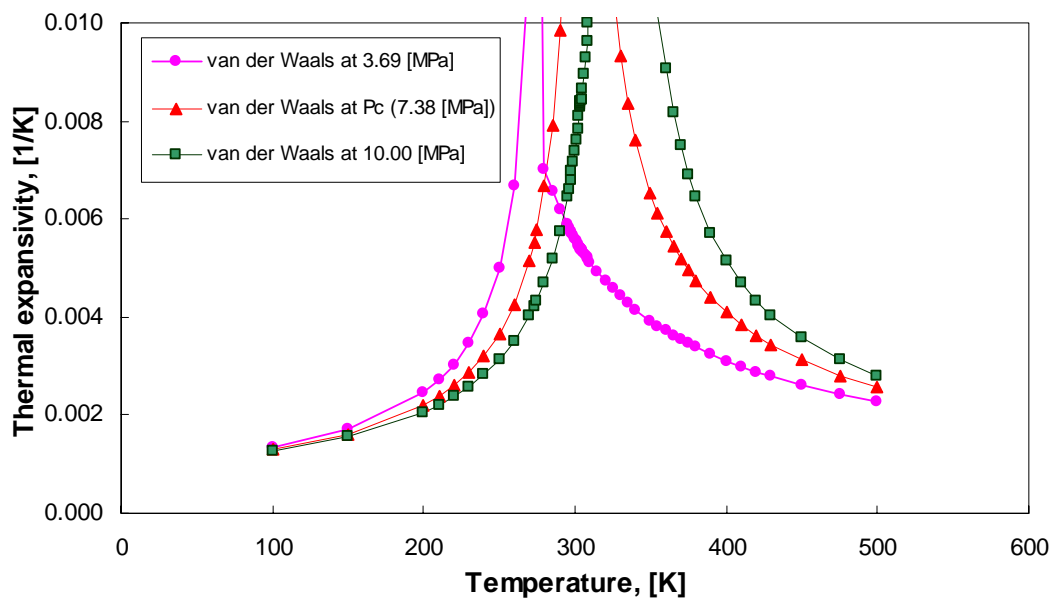


Figure 7.4. Thermal expansion coefficient of carbon dioxide at various pressures.

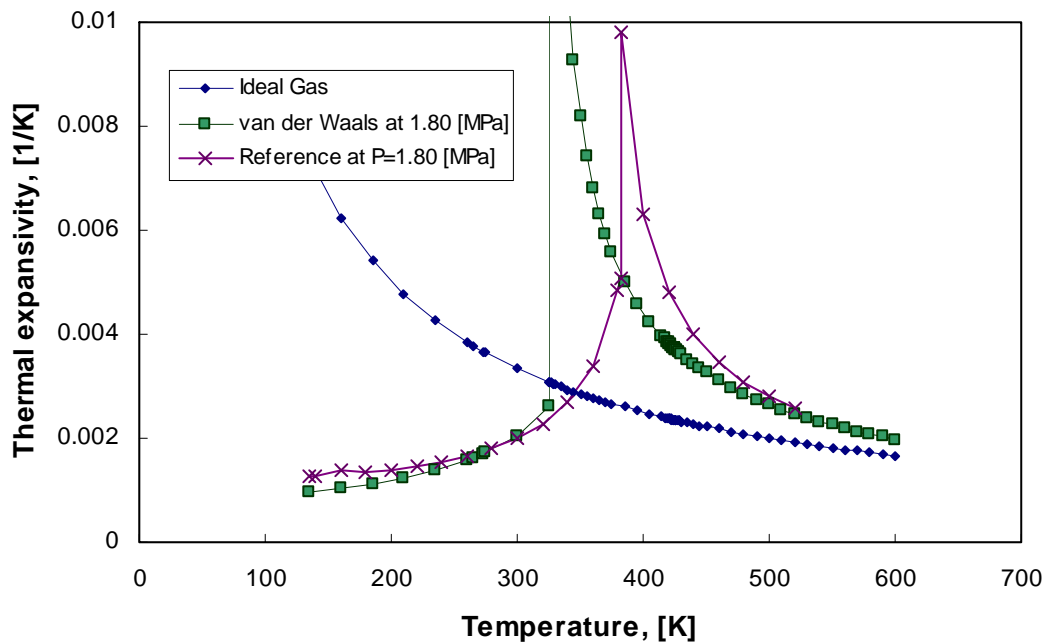


Figure 7.5. Thermal expansion coefficient of butane at 1.80 [MPa].

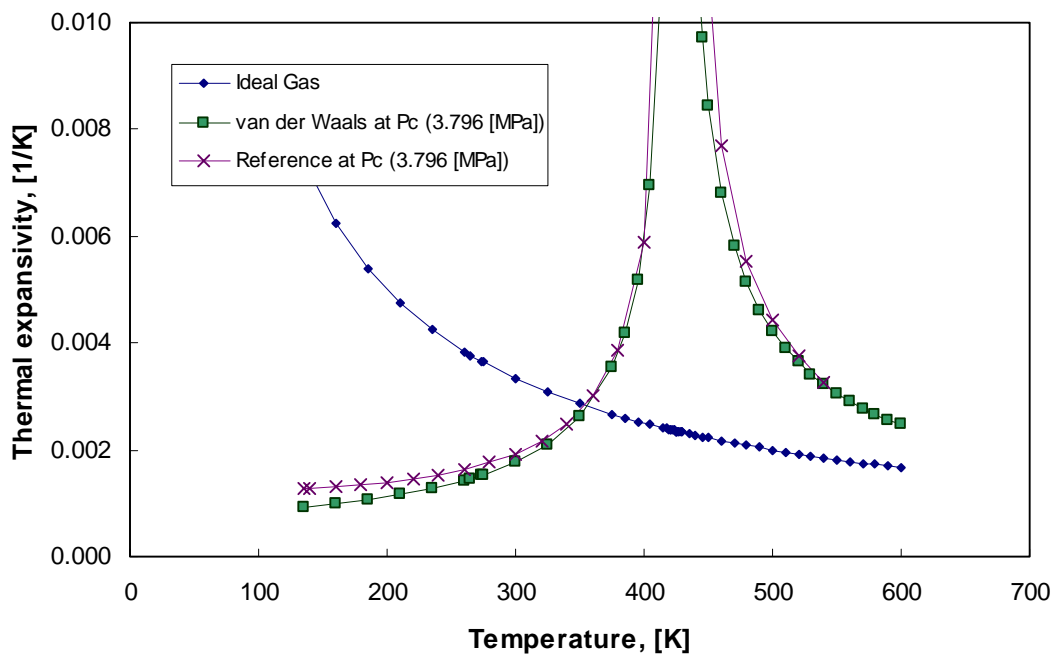


Figure 7.6. Thermal expansion coefficient of butane at its critical pressure.

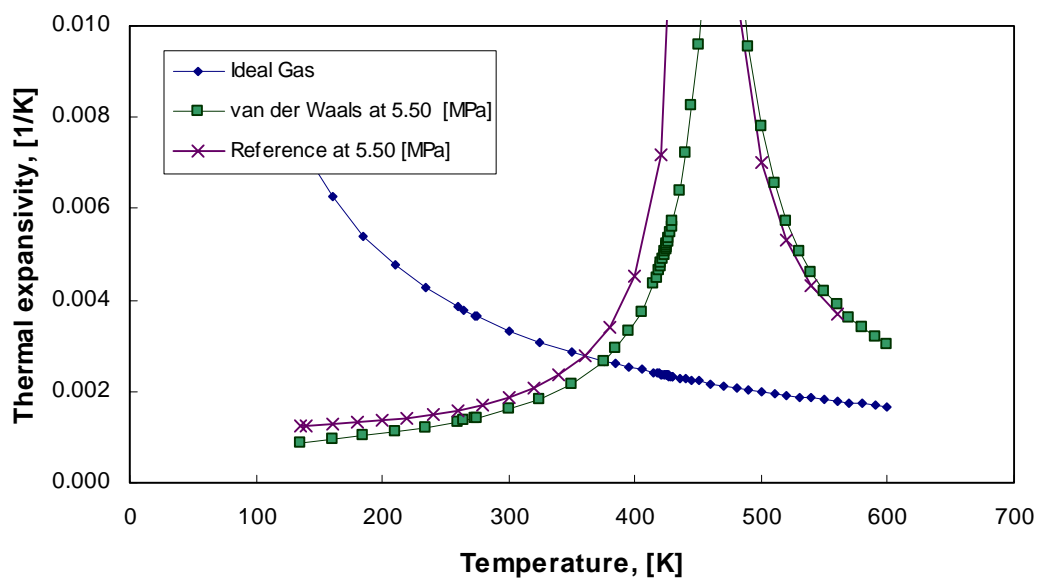


Figure 7.7. Thermal expansion coefficient of butane at 5.50 [MPa].

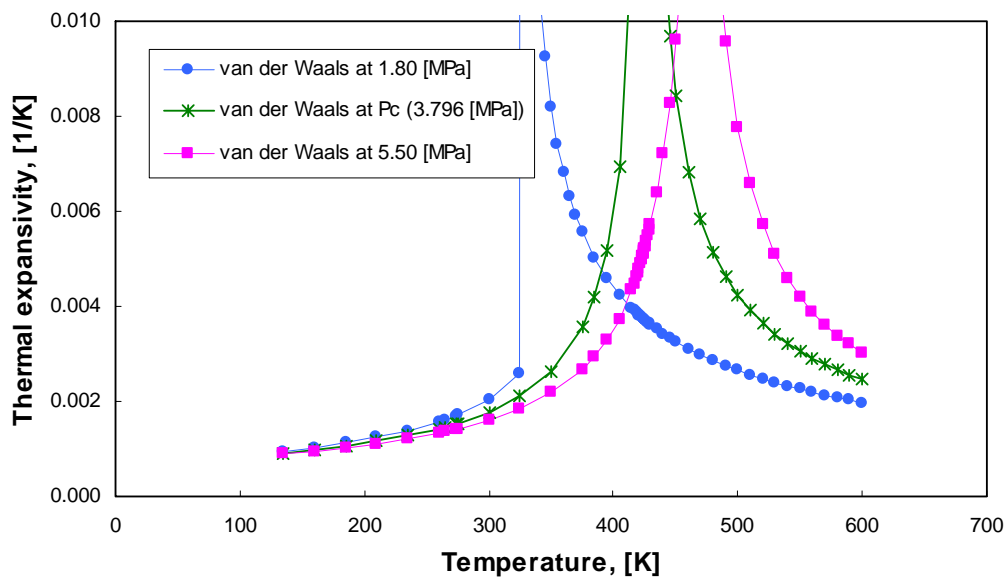


Figure 7.8. Thermal expansion coefficient of butane at various pressures.

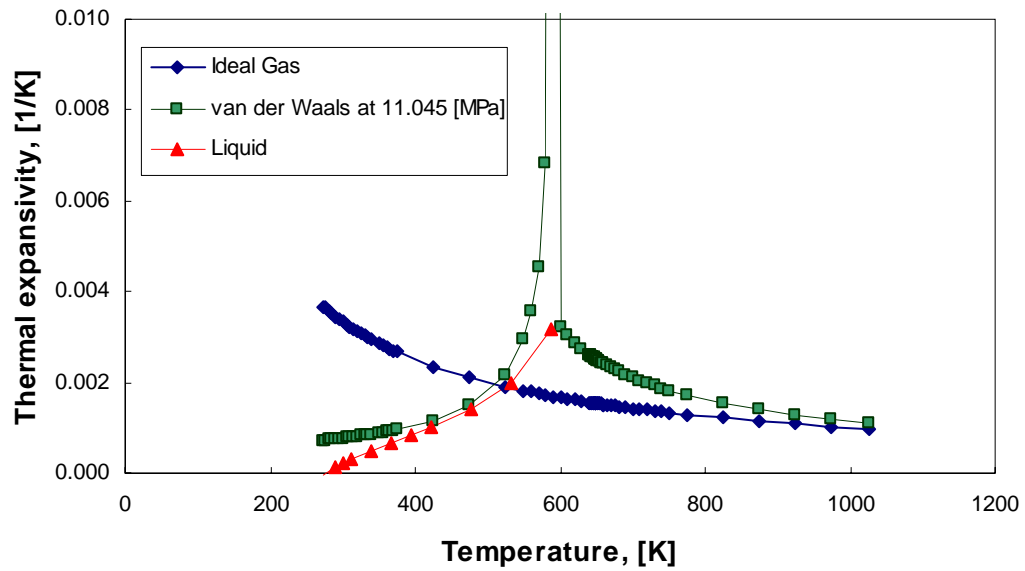


Figure 7.9. Thermal expansion coefficient of water at 11.045 [MPa].

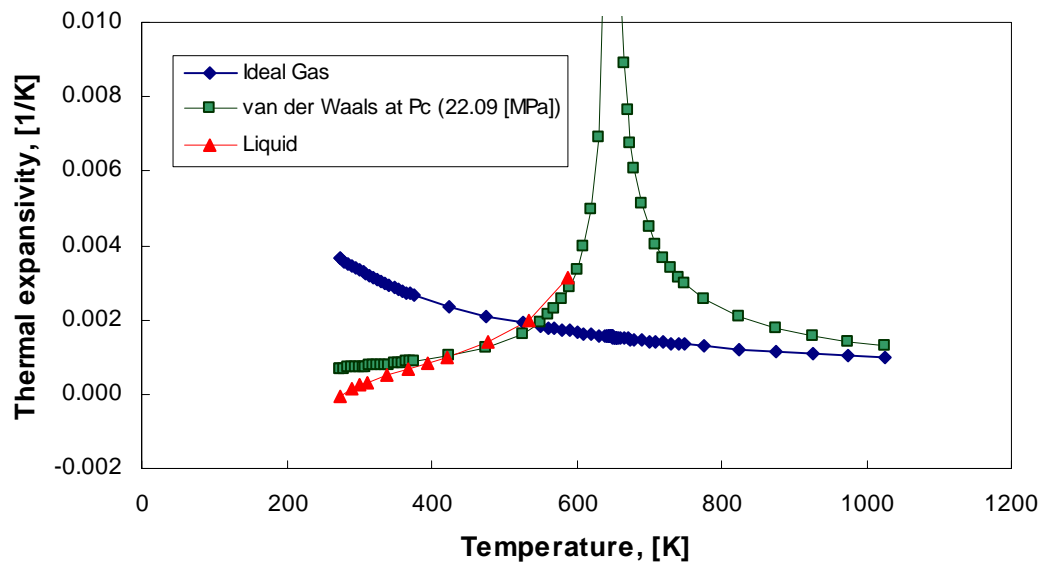


Figure 7.10. Thermal expansion coefficient of water at its critical pressure.

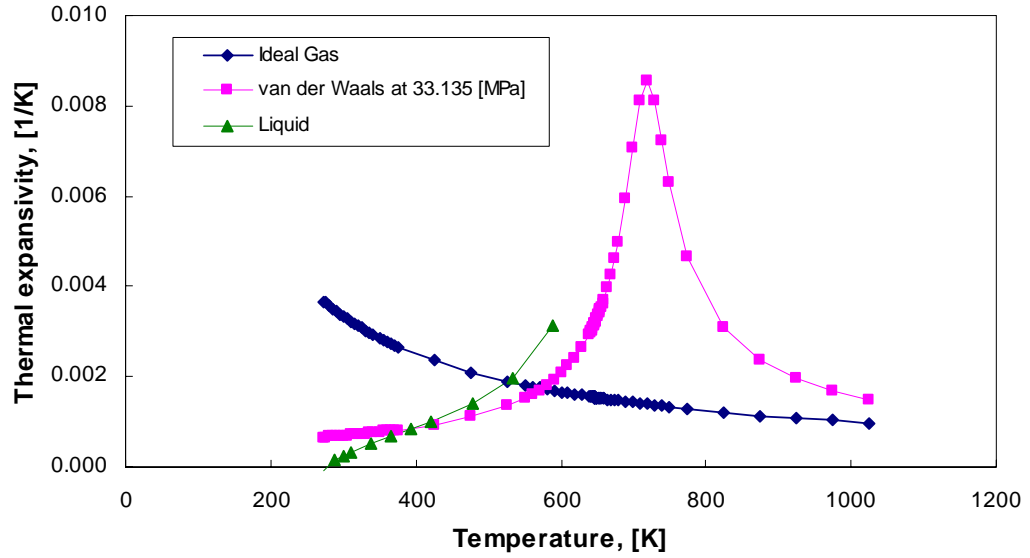


Figure 7.11. Thermal expansion coefficient of water at 33.135 [MPa].

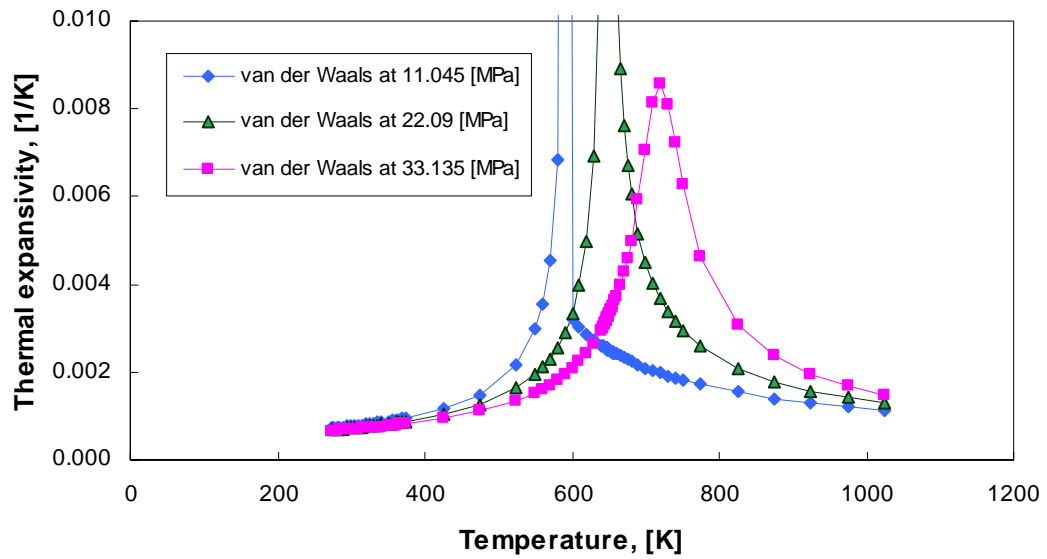


Figure 7.12. Thermal expansion coefficient of water at various pressures.

## 7.2 Heat Transport by Natural Convection

### 7.2.1 Grid Convergence Tests

Before carrying out the final calculations, detailed grid dependency test and code validation studies were performed. The numerical codes for variable and constant thermal expansivity coefficient were used to obtain the figures shown below. A variable grid size in the  $x$ -axis is used for the first 75% of the heated vertical flat plate with the variable step size calculated with Eq. (7.2). Then, a constant step size, calculated with Eq. (7.3), is used for the rest of the plate. In the  $y$ -axis, the grid step size is constant throughout the solution domain and it is calculated with Eq. (7.4).

$$\Delta X = \frac{0.75 X_{max}}{\sum_{i=1}^{100} 1.05^i} \quad (7.2)$$

$$\Delta X_{max} = \Delta X (1.05^{100}) \quad (7.3)$$

$$\Delta Y = \frac{1}{N} \quad (7.4)$$

Table 7.2, shows a summary of the grid convergence tests performed for carbon dioxide as fluid medium at  $P_r = 1.05$  and  $T_r = 1.05$  for variable thermal expansivity coefficient. For all these convergence test the following results were constants: the length of the plate is 0.01610 m, the plate temperature is 340.70 K, the free-stream fluid temperature is 298.12 K, the Grashof, Prandtl, and Rayleigh number were also constants,  $Gr = 5.20 \times 10^8$ ,  $Pr = 2.02$  and  $Ra = 1.05 \times 10^9$ . This Rayleigh number indicates that the fluid flow inside the boundary layer is laminar.

Table 7.2. Results of the temperature variation with the grid points

Variable grid points along $x$ -axis ( $i$ )	50	<b>100</b>	150	200	250
Dimensional length in $x(i)$ [m]	0.011446	<b>0.011496</b>	0.011500	0.011500	0.011500
Temperature [K]	313.381	<b>313.435</b>	313.518	313.520	303.520

Table 7.2 shows the temperature variation as a function of the number of grid points along of the plate ( $x$ -axis). This temperature variation is quite small and does not change significantly due to the grid convergence and to the small size of the plate. Also, this table shows that the dimensional length of the plate is almost constant when varying the number of grid points. Therefore, a value of  $i = 100$  was selected as grid points that it corresponds to a value of length of the plate in this point of 0.011496 [m] and a temperature of 313.435 [K]. These values are indicated in bold in Table 7.2 and they were chosen by give the best results to the executing the program. The dimensional length on the  $y$ -axis for this table was of  $8 \times 10^{-5}$  [m] for a value of grid points constant of  $j=25$ . When  $i = 100$  along of the plate, the grid changes from variable step size to constant step size. A value of  $N = 300$  was used for all the computations. The same grid convergence test was performed for the water and butane as fluid medium obtaining similar results as for carbon dioxide.

### 7.2.2 Literature correlation

An empirical correlation was proposed by Churchill and Chu [6] that is applicable over a wide range of Rayleigh numbers. This is:

$$\overline{Nu}_L = 0.68 + \frac{0.670 Ra_L^{1/4}}{\left[1 + (0.492 / Pr)^{9/16}\right]^{4/9}} \quad \text{for } 0 < Ra_L < 10^9 \quad (7.5)$$

Although Eq. (7.5) better accuracy may be obtained for laminar flow and may be applied for constant heat flux, as well as for constant surface temperature. But Eq. (7.5) is given for average Nusselt number and the plots are given in local Nusselt number as function of local Rayleigh Number. Therefore, an equation was calculated for the whole range of laminar flow. The more important details are given below.

Table 7.3 shows the selected values of Prandtl number for each fluid used with Eq. (7.5). These values were selected between a maximum and minimum value of Prandtl number for three fluids through the program runs.

Table 7.3. Prandtl number for analytical equation

Fluid	Prandtl number
carbon dioxide	2.02
butane	2.16
water	1.23

To derivative this equation, the local and average Nusselt numbers are first defined. The local Nusselt number is defined in terms of the local heat-transfer coefficient,  $h_x$ , as

$$\text{Nu}_x = \frac{h_x x}{k} \quad (7.6)$$

and the average Nusselt number is defined in terms of the average coefficient,  $\bar{h}_L$ , and of the length of the plate,  $L$ :

$$\bar{\text{Nu}}_L = \frac{\bar{h}_L L}{k} \quad (7.7)$$

For a rectangular plate, the average heat-transfer coefficient is related to the local heat-transfer coefficient by [9]:

$$\bar{h}_L = \frac{1}{L} \int_0^L h_x dx \quad (7.8)$$

This equation is useful to obtain an analytical expression for  $\bar{h}_L$  when one for  $h_x$  is available. Conversely, if an equation is available for  $\bar{h}_L$ , the local  $h_x$  can be obtained from:

$$h_x \Big|_{x=L} = \frac{d}{dL} (\bar{h}_L L) \quad (7.9)$$

and expressing Eq. (7.9) in terms of the Nusselt number, it follows that

$$\text{Nu}_x \Big|_{x=L} = L \frac{d}{dL} \bar{\text{Nu}}_L \quad (7.10)$$

Using the chain rule:

$$\text{Nu}_x \Big|_{x=L} = L \frac{d\overline{\text{Nu}}_L}{d\text{Ra}_L} \frac{d\text{Ra}_L}{dL} \quad (7.11)$$

then, the derivative of the Rayleigh number with respect  $L$  is:

$$\frac{d\text{Ra}_L}{dL} = \frac{3\text{Ra}_L}{L} \quad (7.12)$$

substituting Eq. (7.12) in Eq. (7.11) gives:

$$\text{Nu}_x \Big|_{x=L} = 3\text{Ra}_L \frac{d\overline{\text{Nu}}_L}{d\text{Ra}_L} \quad (7.13)$$

recalling the following identities:

$$d\overline{\text{Nu}}_L = \overline{\text{Nu}}_L d \ln \overline{\text{Nu}}_L \quad (7.14)$$

$$d\text{Ra}_L = \text{Ra}_L d \ln \text{Ra}_L \quad (7.15)$$

and substituting Eq. (7.14) and Eq. (7.15) into Eq. (7.13) gives:

$$\text{Nu}_x \Big|_{x=L} = 3 \overline{\text{Nu}}_L \frac{d \ln \overline{\text{Nu}}_L}{d \ln \text{Ra}_L} \quad (7.16)$$

Defining

$$m = \frac{d \ln \overline{\text{Nu}}_L}{d \ln \text{Ra}_L} \quad (7.17)$$

and inserting Eq. (7.17) into Eq. (7.16):

$$\text{Nu}_x \Big|_{x=L} = 3m \overline{\text{Nu}}_L \quad (7.18)$$

Using Table 7.1 of reference [8], for  $\overline{\text{Ra}}_L \geq 10^4$ ,

$$m = \frac{1}{4}$$

then

$$\text{Nu}_x \Big|_{x=L} = \frac{3}{4} \overline{\text{Nu}}_L \quad (7.19)$$

and for  $\overline{\text{Ra}}_L < 10^4$ ,

$$0 < m < \frac{1}{4}$$

Now, expressing the derivative of Eq. (7.17) in numerical (central difference) and considering form, two points such as:  $\text{Ra}_{L2} = 1.05 \text{Ra}_L$  and  $\text{Ra}_{L1} = 0.95 \text{Ra}_L$ , gives

$$m = \frac{\ln \overline{\text{Nu}}_{L2} - \ln \overline{\text{Nu}}_{L1}}{\ln \text{Ra}_{L2} - \ln \text{Ra}_{L1}} = \frac{\ln \left( \frac{\overline{\text{Nu}}_{L2}}{\overline{\text{Nu}}_{L1}} \right)}{\ln \left( \frac{\text{Ra}_{L2}}{\text{Ra}_{L1}} \right)} \quad (7.20)$$

Simplifying,

$$m = 9.992 \ln \left( \frac{\overline{\text{Nu}}_{L2}}{\overline{\text{Nu}}_{L1}} \right) \quad (7.21)$$

substituting Eq. (7.21) in Eq. (7.18), this gives

$$\text{Nu}_x \Big|_{x=L} = 29.976 \overline{\text{Nu}}_L \ln \left( \frac{\overline{\text{Nu}}_{L2}}{\overline{\text{Nu}}_{L1}} \right) \quad (7.23)$$

Finally, replacing Eq. (7.5) in Eq. (7.23) and taking the values of Prandtl number from Table 7.3, the local Nusselt number may be expressed for the three fluids as

*For the water*

$$\text{Nu}_x \Big|_{x=L} = 29.976 \left( \frac{0.837 + 0.670 \text{Ra}_L^{1/4}}{1.231} \right) \ln \left( \frac{0.837 + 0.678 \text{Ra}_L^{1/4}}{0.837 + 0.661 \text{Ra}_L^{1/4}} \right)$$

(7.24)

*For the carbon dioxide*

$$\text{Nu}_x \Big|_{x=L} = 29.976 \left( \frac{0.802 + 0.670 \text{Ra}_L^{1/4}}{1.180} \right) \ln \left( \frac{0.802 + 0.678 \text{Ra}_L^{1/4}}{0.802 + 0.661 \text{Ra}_L^{1/4}} \right) \quad (7.25)$$

*For the butane*

$$\text{Nu}_x \Big|_{x=L} = 29.976 \left( \frac{0.798 + 0.670 \text{Ra}_L^{1/4}}{1.174} \right) \ln \left( \frac{0.798 + 0.678 \text{Ra}_L^{1/4}}{0.798 + 0.661 \text{Ra}_L^{1/4}} \right) \quad (7.26)$$

Equations (7.24), (7.25) and (7.26) are empirical correlations use to generate curves to be compared to those obtained by the numerical code in graphs of Nusselt versus Rayleigh number.

### 7.2.3 Results

The Nusselt number values computed as a function at the Rayleigh number for supercritical carbon dioxide and variable thermal expansivity coefficient are shown in Fig. 7.13. The simulations were performed at  $P_r = 1.05$  and values of  $T_r$  of 1.00, 1.05 and 1.10. The results of these simulations are plotted in logarithmic scale so the curves approach straight lines. The first line at  $T_r = 1.00$ , stands alone way above the rest. This is most likely because it is at the critical temperature and at a pressure near the critical point. This line exhibits some oscillations due to the transition from sub critical to supercritical region. The next two lines down are results of the simulations at the same pressure and increasing reduced temperature from  $T_r = 1.05$  to  $T_r = 1.10$ . The fourth line was computed at far-from-critical

conditions. The curve corresponds to the empirical correlation; values were computed with Eq. (7.25).

Figure 7.14 shows  $Nu_x$  as a function of  $Ra_x$  for butane at constant  $P_r$  and different values of  $T_r$ . The same trend shown in Fig. 7.13 is observed here, except for the line at  $P_r = 1.05$  and  $T_r = 1.00$  (critical temperature) that presents more noise for  $Ra_x < 10^4$ . This type of noise is more likely to occur at or very close to the critical temperature. The behavior observed in Fig. 7.15 is similar to that in Fig. 7.13. In all the cases, the numerical calculations are compared to the empirical correlation. Finally, it is important to observe in Figs. 7.13, 7.14, and 7.15, that the higher the temperature, the closer the lines are to that representing the empirical correlation. Here, the effect of the temperature on the local heat-transfer coefficient can be seen.

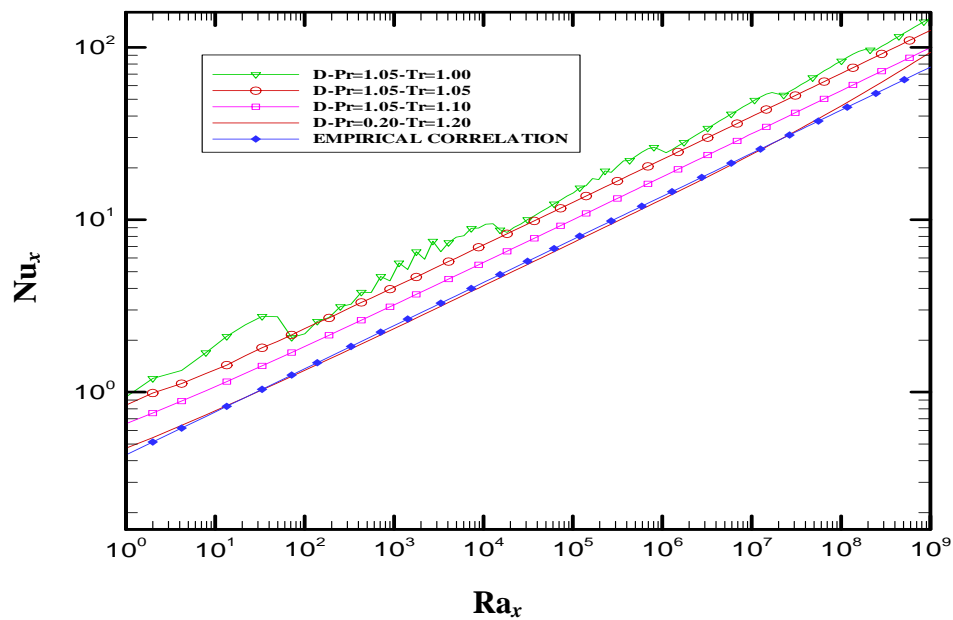


Figure 7.13.  $Nu_x$  as a function of  $Ra_x$  for carbon dioxide at  $Pr = 1.05$ .

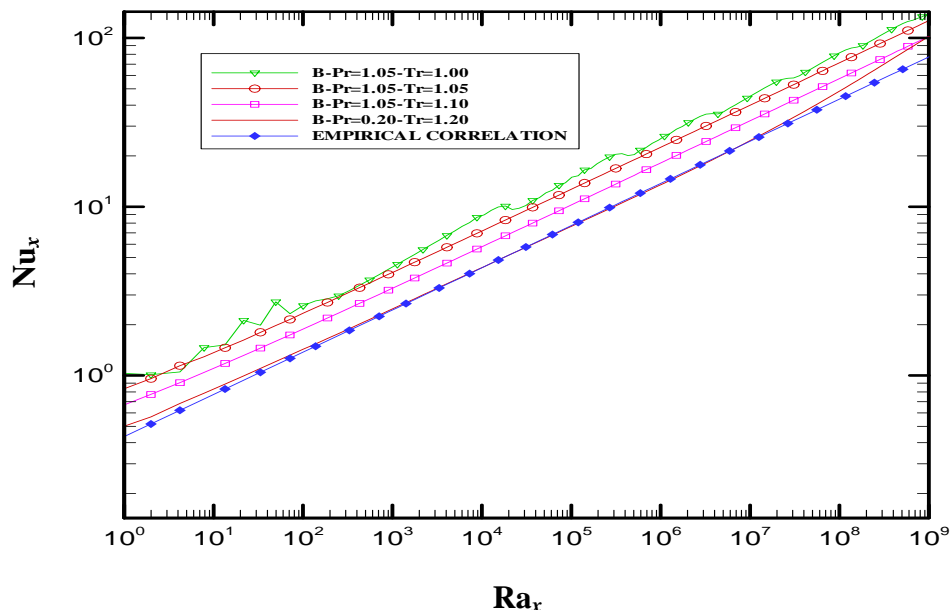


Figure 7.14.  $Nu_x$  as a function of  $Ra_x$  for butane at  $Pr = 1.05$ .

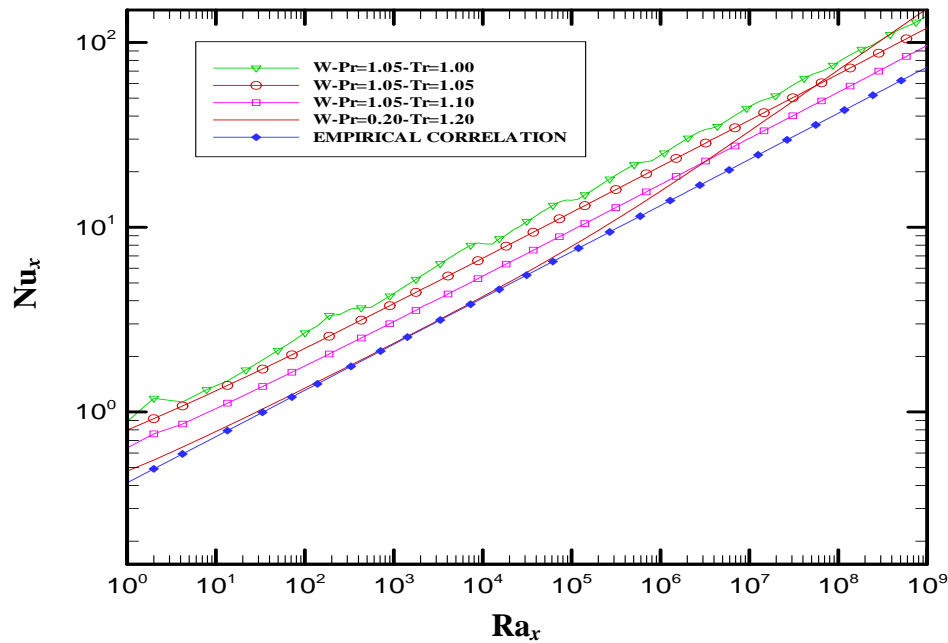


Figure 7.15.  $Nu_x$  as a function of  $Ra_x$  for water at  $P_r = 1.05$ .

Numerical computations were also carried at variable pressure and constant temperature. Fig. 7.16 shows the local Nusselt number as a function of  $Ra_x$  for carbon dioxide at  $T_r = 1.05$  and reduced pressure of 1.05, and 1.10. Note that these two lines are almost superimposed. Therefore, it can be concluded that the effect of the pressure is not significant. Additionally, a line at conditions removed from the critical point ( $P_r = 0.20$  and  $T_r = 1.20$ ), has been included. This line happens to be away from the other two lines and closer to the empirical correlation line. Similar trends are observed in Fig. 7.17 for butane and in Fig. 7.18 for water.

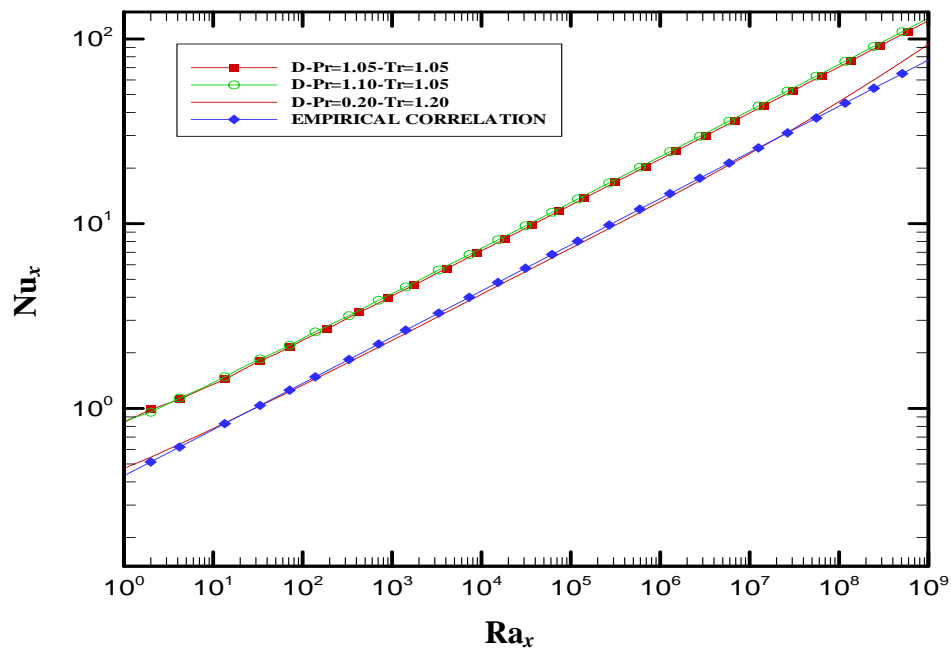


Figure 7.16.  $Nu_x$  as a function of  $Ra_x$  for carbon dioxide at  $T_r=1.05$ .

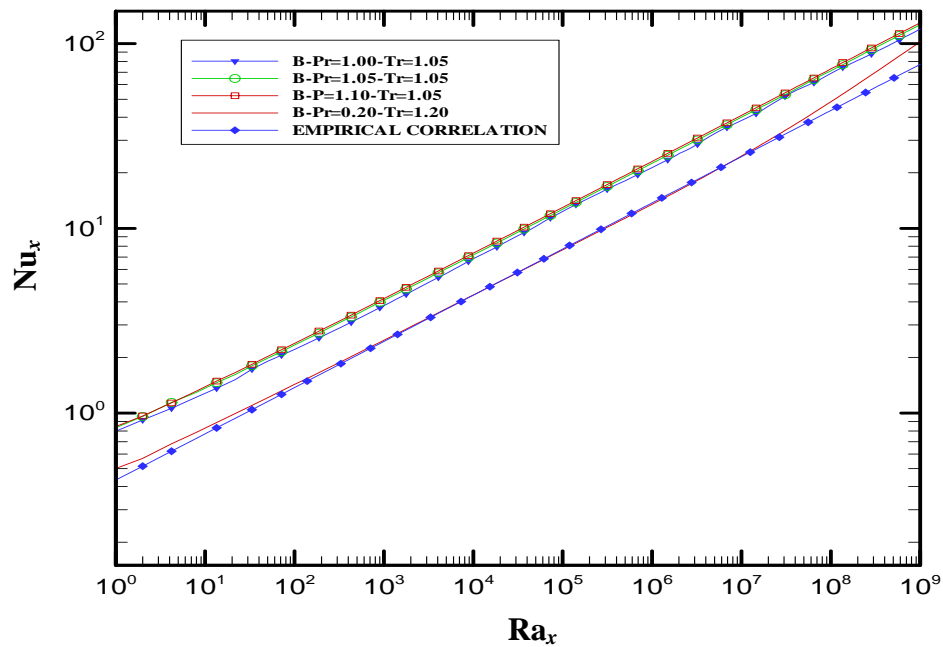


Figure 7.17.  $Nu_x$  as a function of  $Ra_x$  for butane at  $T_r=1.05$ .

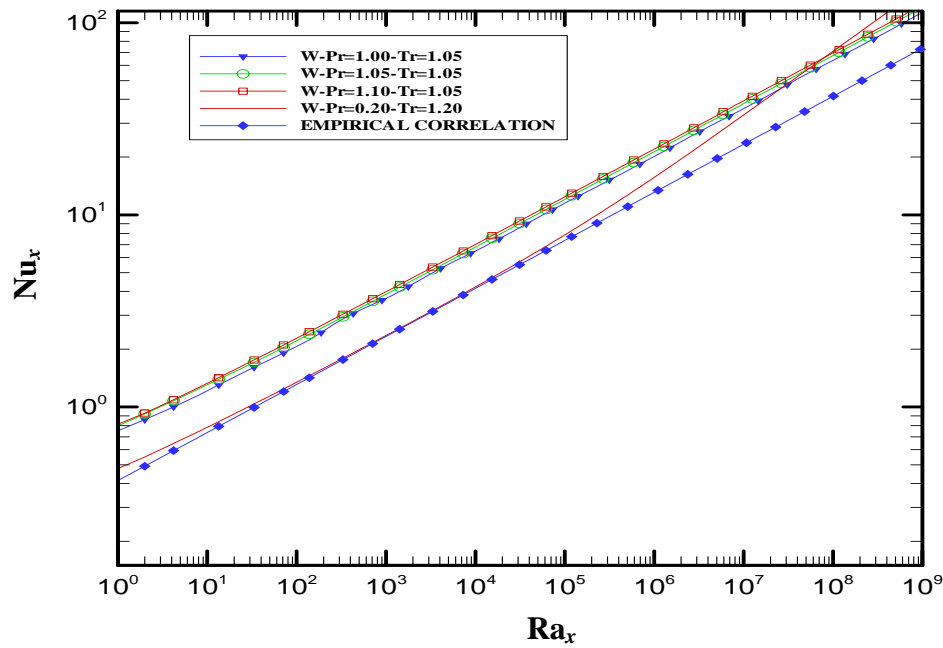


Figure 7.18.  $Nu_x$  as a function of  $Ra_x$  for water at  $T_r=1.05$ .

For illustration purposes, the velocity profiles for variable and constant thermal expansivity for water, at an arbitrarily chosen value of  $x$ , are plotted in Fig. 7.19. The values of  $u$  were obtained at  $x = 0.02176$  [m] for  $P_r = 1.05$  and  $T_r = 1.05$ . The Prandtl number computed by the numerical code is 1.23 and is in good agreement with the given values for supercritical water. The numerical simulation also gives: the wall temperature,  $T_w = 724.80$  [K]; the fluid temperature,  $T_f = 634.20$  [K]; the total length of the plate,  $L = 0.03047$  [m] and the local Rayleigh number,  $Ra_x = 1.05 \times 10^9$ . Note that the velocity profile with variable thermal expansivity has a velocity maximum much higher than the one with

constant thermal expansivity. Also, at that point the thickness of the boundary layer for variable thermal expansivity is lower than that for constant thermal expansivity.

Figure 7.20 shows the temperature profiles at the same conditions of Fig. 7.19. This figure confirms that the boundary layer for variable thermal expansivity is thinner than the one for constant thermal expansivity. It should also be noted that the agreement is very good if the velocity and temperature profiles obtained with numerical code at constant thermal expansivity are compared to given those in the classical books.

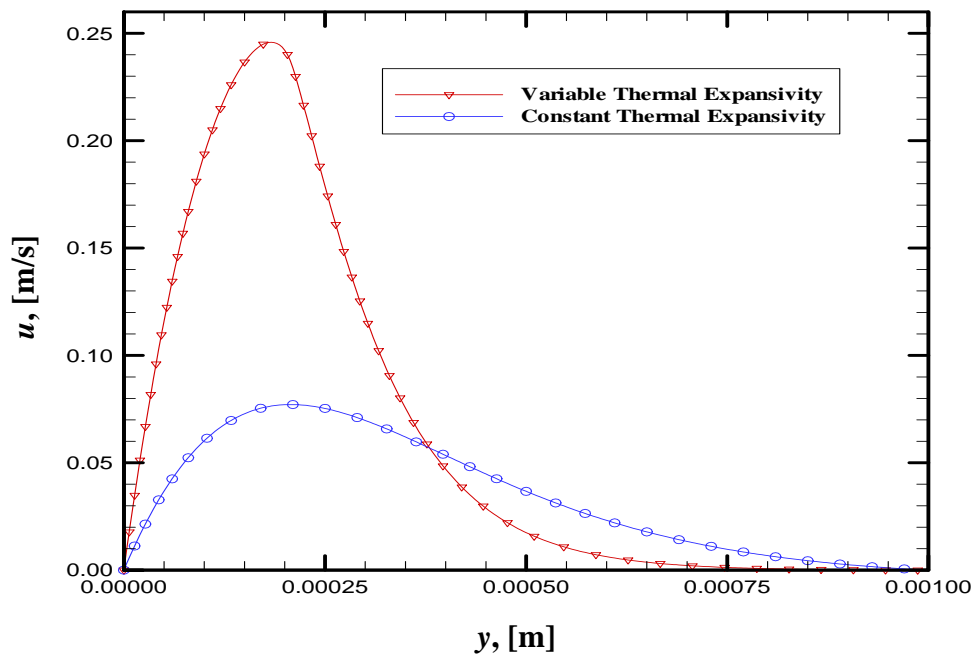


Figure 7.19. Dimensional velocity profile for water at  $x = 0.02176$  [m],  $P_r = 1.05$ , and  $T_r = 1.05$ .

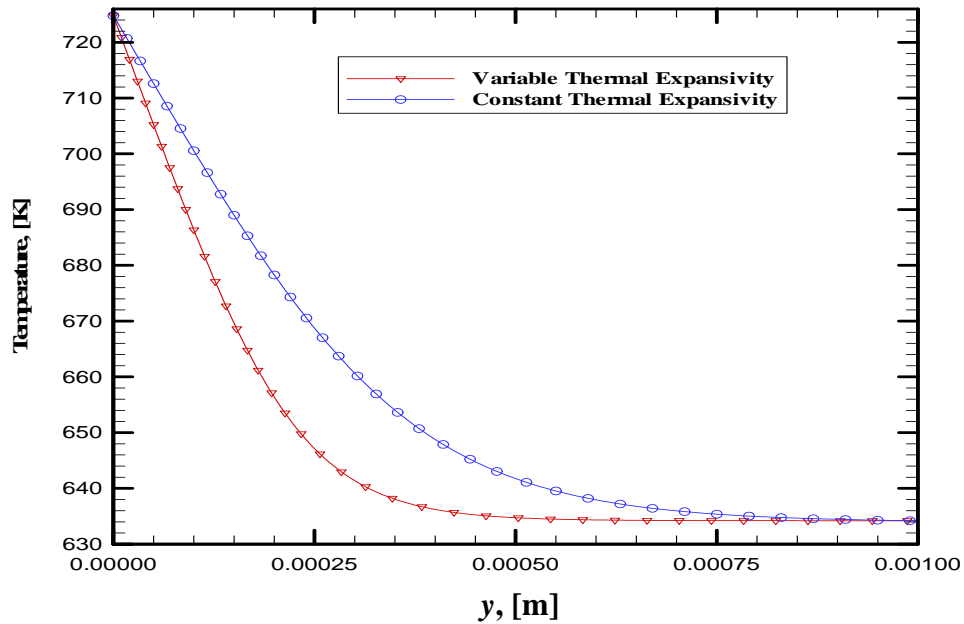


Figure 7.20. Dimensional temperature profile for water at  $x = 0.02176$  [m],  $P_r = 1.05$ , and  $T_r = 1.05$ .

Finally, nice velocity contour lines for water at  $P_r = 1.05$  and  $T_r = 1.05$ , are presented in Fig. 7.21. These contour lines were computed along the entire plate and in the whole domain of solution in the  $y$ -direction. The velocity maximum is at the heart of all these lines and the velocity gradually approaches zero, the velocity outside the boundary layer.

Figure 7.22 shows the temperature contour lines for the water at the same conditions as in Fig. 7.21. The temperature gradually decreases from  $T_w = 724.80$  [K] to  $T_\infty = 634.20$  [K]. The results shown in Figs. 7.21 and 7.22 were obtained with variable thermal expansivity, using Tecplot Software.

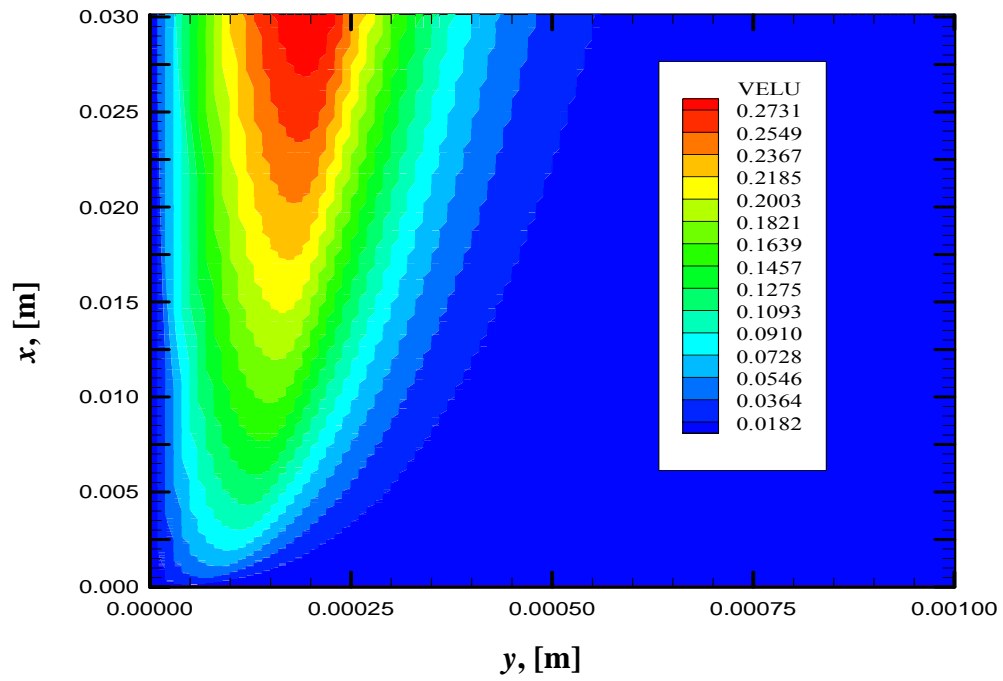


Figure 7.21. Velocity contour line for water at  $P_r = 1.05$  and  $T_r = 1.05$ .

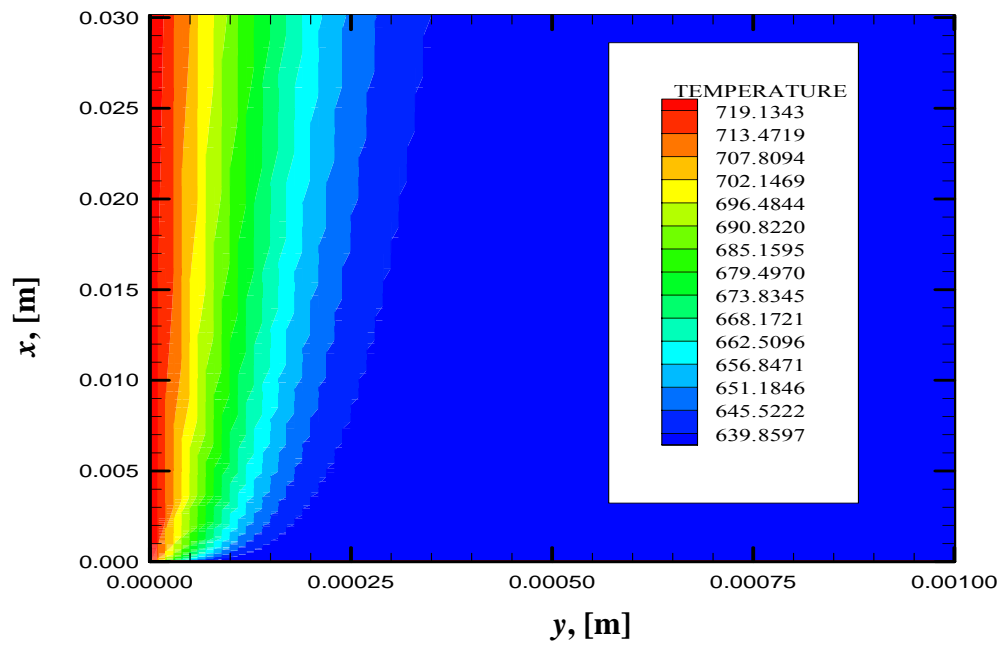


Figure 7.22. Temperature contour lines for water at  $P_r = 1.05$  and  $T_r = 1.05$ .

## CHAPTER 8

### CLOSURE

#### 8.1 Conclusions

##### 8.1.1 Thermodynamic Model

A thermodynamic model has been developed to represent the thermal expansivity of real fluids based on an equation-of-state approach. This model has been further developed for the van der Waals EOS, and used to calculate the isobars of  $\beta$  versus  $T$  for three fluids normally used as supercritical solvents and compared to values computed for accurate density values. It is concluded that this approach produces very good results even when a simple EOS such as the van der Waals EOS is used.

This contribution is important in various regards. First, in any practical application of supercritical-fluid extraction where heat transfer plays a role, the effect of free convection has to be taken into account because of the huge enhancement of this phenomenon in the supercritical region of the solvent. Second, when developing a model or correlation for free convection, it is normally assumed that  $\beta$  is a constant. In view of the results presented here, when working near the critical point of the solvent this assumption is no longer true.

### **8.1.2 Numerical Model**

A numerical model was developed for the analysis of the free-convection flow about a heated vertical flat plate with variable thermal expansivity coefficient. Three fluids were used to perform the numerical simulations: carbon dioxide, butane, and water. The equation for the thermal expansivity coefficient obtained through the thermodynamic model was used in the momentum equation. A numerical code was used to solve the coupled boundary layer equations.

Velocity and temperature profiles were plotted obtaining excellent results. Also velocity and temperature profiles were plotted at constant thermal expansivity showing good agreement with the existent literature value. The results were expressed in terms of dimensionless numbers as local Nusselt and Rayleigh numbers. It was found that at constant pressure the lines obtained approach the line computed with the empirical correlation, it can be seen with the increases temperature. Finally, it was found that at constant temperature these lines are almost superimposed suggesting that the effect of pressure is weak.

## **8.2 Suggestions for Future Work**

Possible extensions to the present work that are pertinent to the issues discussed in this thesis, are:

- An experimental validation of the numerical solution of this study is highly desirable to verify the numerical simulation.
- To gain a better physical insight in natural convection in supercritical fluids, experiments can be performed with different type of geometries.
- This study could be extended to other type of heat transfer such as in forced convection flow and heat transfer in supercritical fluids at turbulent flow.

### 8.3 Bibliography

- [1] Arai, Y., Sako, T., Takebayashi, Y.; 2001; *Supercritical Fluids-Molecular Interactions, Physical Properties and New Applications*. First Edition, Springer, Berlin, Germany.
- [2] Angus, S.; B. Armstrong, B.; Reuck, K.; 1976; *International Thermodynamic Tables of the Fluid State-Carbon Dioxide*. First Edition, Pergamon Press, Headington Hill Hall, Oxford OX3 0BW, England.
- [3] Bejan, A.; 1984; *Convection Heat Transfer*. First Edition, Wiley, New York, NY.
- [4] Bird, R., B.; Stewart, W.; Lightfoot, E.; 1960; *Transport Phenomena*. Wiley, New York, NY.
- [5] Constantinides, A.; Mostoufi, N.; 1999; *Numerical Methods for Chemical Engineers with MATLAB Applications*. First Edition, Prentice-Hall PTR, New Jersey, NJ.
- [6] Churchill, S. W. and H. H. S. Chu; 1975; "Correlation Equations for Laminar and Turbulent Free Convection from a Vertical Plate," *Int. J. Heat Mass Transfer*, 18, 1323.
- [7] Haynes, W., M.; Goodwin, R., D.; 1982; *Thermophysical Properties of Normal Butane from 135 to 700 K at Pressures to 70 MPa*. U.S. Department of Commerce. U.S. Government Printing Office. Washington, DC.
- [8] Holman, J. P.; 1981; *Heat Transfer*. Fifth Edition, McGraw-Hill Book Company, New York, NY.
- [9] Incropera, F. P., DeWitt, D. P.; 1981; *Fundamentals of Heat Transfer*. First Edition, John Wiley & Sons, Inc, New York, NY
- [10] Kakac, S.; Aung, W.; Viscanta, R.; 1985; *Natural Convection: Fundamentals and Applications*. Hemisphere Publishing Corp., New York, NY.
- [11] Kakarala, C. R.; Thomas, L. C.; 1980; "Turbulent Combined Forced and Free Convection Heat Transfer in Vertical Tube Flow of Supercritical fluids," *Int. J. Heat & Fluid Flow*, 2, 3.

- [12] Keenan, J., H.; Keyes, F., G.; Hill, P., G.; Moore, J., G.; 1969; *Steam Tables*. Wiley, New York, NY.
- [13] Lee, B. I., and Kesler, M. G.; 1975; *AIChE J.*, 21:510
- [14] McHugh, M. A., Krukonis, V. J.; 1994; *Supercritical Fluid Extraction: Principles and Practice*. Butterworth-Heinemann.
- [15] Montgomery, D. C.; 2001; *Design & Analysis of Experiments*. Fifth Edition, Wiley, New York, NY.
- [16] Müller, E., A.; Estévez, L., A.; 1990. "Mixing Expansivities and Grashof Number in Supercritical Fluids Using Cubic Equations of State" *J. Supercrit. Fluids*, 3, 136-142.
- [17] Müller, E., A.; Olivera-Fuentes, C., and Estévez, L., A.; 1989; "General Expressions for Multicomponent Fugacity Coefficients and Residual Properties from Cubic Equations of State," *Lat. Am. Appl. Res.*, **19**, 99-109.
- [18] Nishikawa, K.; Ito, T.; Yamashita, H.; 1973; "Free-Convective Heat Transfer to a Supercritical fluid," *J. of Heat Transfer*.
- [19] Nishikawa, K.; Ito, T.; 1969; "An analysis of Free-Convective Heat Transfer from an Isothermal Vertical plate to Supercritical fluid," *Int. J. Heat Mass Transfer*, 12, 1449-1463.
- [20] Oosthuizen, P.; Naylor, D.; 1999; *An Introduction to Convective Heat Transfer Analysis*. First Edition, McGraw-Hill, New York, NY.
- [21] Ostrach, S.; 1952; An Analysis of Laminar Free-Convection Flow and Heat Transfer about a Flat Plate Parallel to the Direction of the Generating Body Force. Report 1111- Supersedes NACA TN 2635.
- [22] Poling, B., Prausnitz, J., O'Connell, J.; 2001; *The Properties of Gases and Liquids*. Fifth Edition, McGraw-Hill, New York, NY.
- [23] Plawsky, J., L.; 2001; *Transport Phenomena Fundamentals*. Marcel Dekker, New York, NY.
- [24] Reid, R., Prausnitz, J., Poling, B.; 1987; *The Properties of Gases and Liquids*. Fourth Edition, McGraw-Hill, New York, NY.
- [25] Schmidt, G.; Wenzel, H.; 1980; *Chem. Eng. Sci.* 35, 1503.

[26] Stiel, L. I., and Thodos, G.; 1964; *AIChE J.*, 10:26.

[27] Welty, J.; Wicks, C.; Wilson, R.; 1984; *Fundamentals of Momentum, Heat, and Mass Transfer*. Third Edition, Wiley, New York, NY.

## Appendix A

### Analytical Solution for Cubic Polynomial Equations

This Appendix presents the analytical solutions  $x_1$ ,  $x_2$  and  $x_3$  for a cubic polynomial equation written as:

$$x^3 + p_1x^2 + p_2x + p_3 = 0 \quad (\text{A.1})$$

$$\text{Let } Q = \frac{3p_2 - p_1^2}{9}; \quad R = \frac{9p_1p_2 - 27p_3 - 2p_1^3}{54}; \quad D^* = Q^3 + R^2$$

$D^*$  is called the discriminant and its value determines the domain of the roots to Eq. (A-1): (1) If  $D^* < 0$ , all roots are real and unequal; (2) if  $D^* = 0$ , all roots are real and at least two are equal; and (3) if  $D^* > 0$ , only one root is real and two are conjugate complex.

$$\underline{D^* > 0}$$

For  $D^* > 0$ , the real root is given by

$$x_1 = S + T - \frac{1}{3}p_1 \quad (\text{A.2})$$

and the two complex roots are ( $i = \sqrt{-1}$ ):

$$x_{2,3} = -\frac{1}{2}(S + T) - \frac{1}{3}p_1 \pm \frac{1}{2}i\sqrt{3}(S - T) \quad (\text{A.3})$$

where

$$S = \left(R + \sqrt{D^*}\right)^{1/3} \quad \text{and} \quad T = \left(R - \sqrt{D^*}\right)^{1/3}$$

$$\underline{D^* = 0}$$

If  $D^* = 0$ ,  $S = T$  and the imaginary parts vanish, so 3 real roots result. These are:

$$x_1 = 2S - \frac{1}{3}p_1 \quad (\text{A.4})$$

$$x_2 = x_3 = -S - \frac{1}{3}p_1 \quad (\text{A.5})$$

$$\underline{D^* < 0}$$

For  $D^* < 0$ , the roots are given by:

$$x_1 = 2\sqrt{-Q} \cos\left(\frac{\theta}{3}\right) - \frac{1}{3}p_1 \quad (\text{A.6})$$

$$x_2 = 2\sqrt{-Q} \cos\left(\frac{\theta}{3} + 120^\circ\right) - \frac{1}{3}p_1 \quad (\text{A.7})$$

$$x_3 = 2\sqrt{-Q} \cos\left(\frac{\theta}{3} + 240^\circ\right) - \frac{1}{3}p_1; \quad (\text{A.8})$$

where  $\cos \theta = \frac{R}{\sqrt{-Q^3}}$

## Appendix B

### Heat Capacity

Figure B.1 shows the inverse of the heat capacity as a function of the reduced pressure for carbon dioxide [24]. It can be seen that when the temperature increases, the inverse of the heat capacity increases. At the critical point the inverse of the heat capacity goes to zero. The same is true for the butane and water in Figs. B.2 and B.3. Therefore, using these figures, values of the heat capacity that are not obtained from Eq. 6.9 were interpolated.

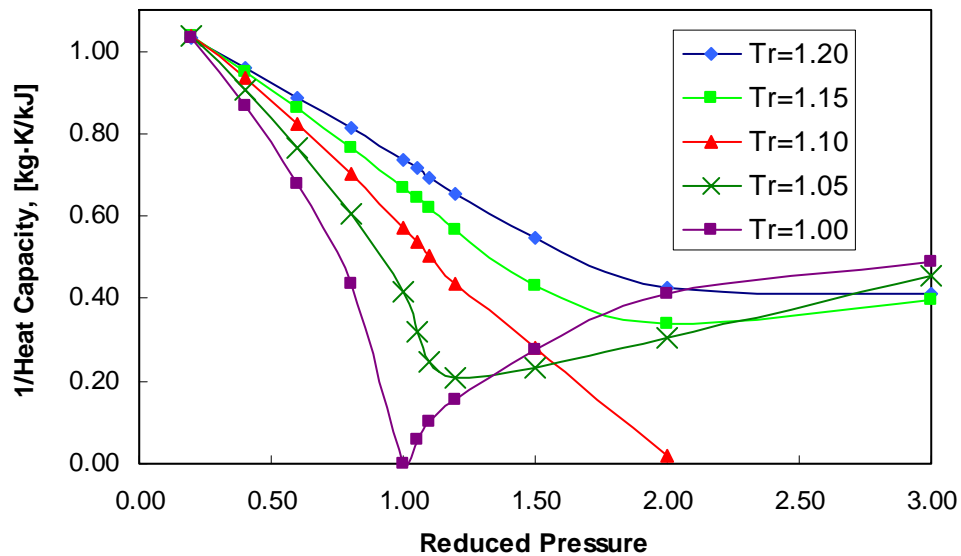


Figure B.1. Inverse of the heat capacity of carbon dioxide as a function of reduced pressure and temperatures.

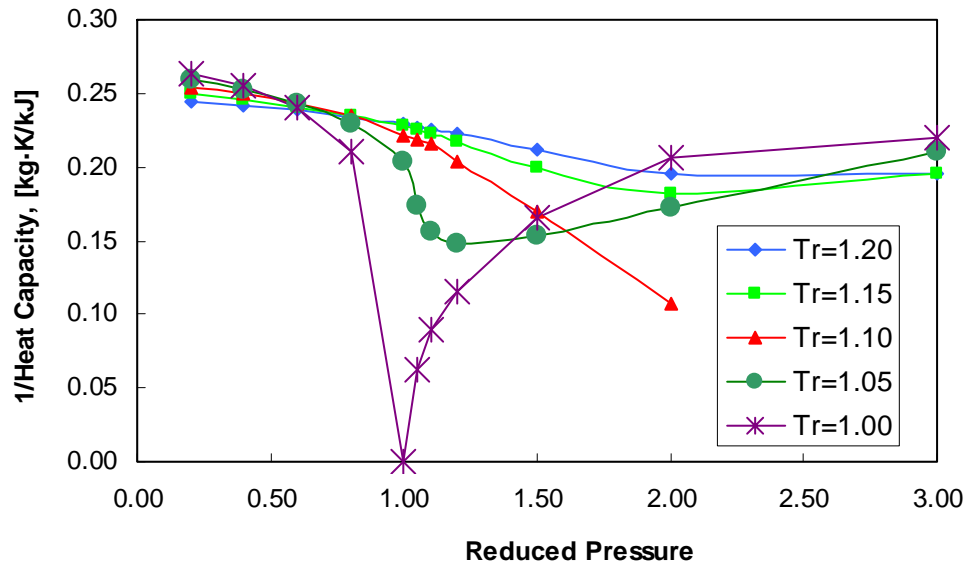


Figure B.2. Inverse of the heat capacity of butane as a function of reduced pressure and temperatures.

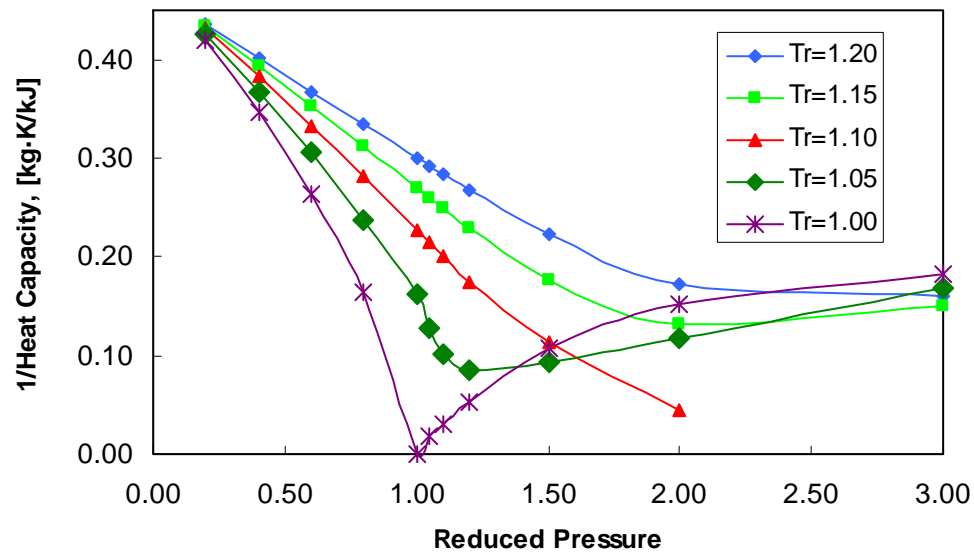


Figure B.3. Inverse of the heat capacity of water as a function of reduced pressure and temperatures.

## Appendix C

### Numerical Code

```
!*****
! THIS PROGRAM SOLVES THE NATURAL CONVECTIVE
! LAMINAR BOUNDARY LAYER FLOW OVER A VERTICAL
! SURFACE USING THE FINITE DIFFERENCE TECHNIQUE WITH
! AN UNDER-RELAXATION ITERATIVE PROCEDURE.
!*****

      DIMENSION U(2,300),V(2,300),T(2,300),A(300),B(300)
      DIMENSION C(300),D(300),Y(300),H(300),BET(300),BETD(300)
      DIMENSION XX(600),VELU(600,600),VELV(600,600),TEMP(600,600)
      DIMENSION COEF(600),NU(600),GRX(600),RAX(600),FIXP(20,20)
      REAL MW, K, G, NU,COEFP,NUP,SUM,KO
      INTEGER LOP
      CHARACTER NAMEFILE*25
      COMMON IONE,ITHREE
      DOUBLE PRECISION DY, Y, DX, DXMAX
      IONE=0
      ITHREE=0

!*****
      OPEN(1,FILE='LAMB NAT.TXT')
      OPEN(2,FILE='LAMB NAT2.TXT')
      OPEN(3,FILE='LAMB NAT3.TXT')
      OPEN(8,FILE='BLFIELD.TXT')
      OPEN(9,FILE='BLFIELD2.TXT')

!*****

!           PRE-PROCESSING: INPUT DATA

!*****

!  ASSIGN KNOWN VALUES

!  UNIVERSAL CONSTANTS

      R=8.314           ! UNIVERSAL CONSTANT OF GASES, [J/mol·K]
      GR=9.81          ! ACCELERATION OF GRAVITY, [m/s^2]

!  RUN REDUCED FILM CONDITIONS (USED FOR FLUID PROPERTIES)
!  PROBLEM VARIABLES

      W=0.0010         ! WIDTH OF THE SOLUTION DOMAIN, [m]
      DELTATR=0.14
      TRE=1.0          ! REDUCED FILM TEMPERATURE
```

```

PRE=1.0      ! REDUCED FILM PRESSURE

WRITE(*,*)'INPUT TYPE OF FLUID:'
WRITE(*,*)'1=CARBON DIOXIDE'
WRITE(*,*)'2=BUTANE'
WRITE(*,*)'3=WATER'

READ(*,*)LOP

IF(LOP.EQ.1) THEN
    NAMEFILE='CPCARBONDIOXIDE.TXT'
ELSE IF(LOP.EQ.2) THEN
    NAMEFILE='CPBUTANE.TXT'
ELSE
    NAMEFILE='CPWATER.TXT'
END IF

WRITE(*,*)NAMEFILE ! CONTAINS MATRIX WITH FLUID PROPERTIES
WRITE(*,*)'

OPEN(12,FILE=NAMEFILE,STATUS='OLD')

! FIRST 11 ROWS CONTAIN CP AT PREESTABLISHED CONDITIONS:
! ROWS   : PR1=0.20, PR2=0.40, PR3=0.60, PR4=0.80, PR5=1.00, PR6=1.05,
!         PR7=1.10, PR8=1.20, PR9=1.50, PR10=2.00, PR11=3.00

! COLUMNS: TR1=1.20, TR2=1.15, TR3=1.10, TR4=1.05, TR5=1.00

N1=12          ! NUMBER OF ROWS OF THE MATRIX
M1=5           ! NUMBER OF COLUMNS OF THE MATRIX

DO I1=1,N1
    READ(12,*)(FIXP(I1,J1),J1=1,M1)
END DO

NN1=5          ! ROW OF THE SEARCH VALUE
MM1=5          ! COLUMN OF THE SEARCH VALUE

CP=FIXP(NN1,MM1) ! HEAT CAPACITY, [J/kg·K]

! ROW 12 CONTAINS THE FOLLOWING PROPERTIES OF THE FLUID

TC=FIXP(N1,1)  ! CRITICAL TEMPERATURE OF FLUID, [K]
PC=FIXP(N1,2)  ! CRITICAL PRESION OF FLUID, [Pa]
ZC=FIXP(N1,3)  ! CRITICAL COMPRESSIBILITY FACTOR
VC=FIXP(N1,4)  ! CRITICAL VOLUME, [m^3/mol]
MW=FIXP(N1,5)  ! MOLECULAR WEIGHT, [kg/mol]

! END INPUT DATA
! CALCULATION OF DIMENSIONAL RUN CONDITIONS
DELTAT=DELTATR*TC
TA=TRE*TC      ! AVERAGE TEMPERATURE OF FLUID, [K]

```

```

P=PRE*PC          ! PRESSURE OF THE FLUID, [Pa]
TW=TA+DELTAT/2.  ! WALL TEMPERATURE, [K]
TF=TA-DELTAT/2. ! FLUID TEMP. OUTSIDE BOUNDARY LAYER, [K]

CALL ZETA (P,TA,PC,TC,ZV,ZL,IROOT)

! ESTIMATION OF KINEMATIC VISCOSITY
! FIGURE 9-6, PAGE 9.32 OF POLING ET AL. (2001)

DENS=MW*P/(ZV*R*TA)      ! DENSITY, [kg/m^3]
ETAEX=0.88                ! DIMENSIONLESS PARAMETER
EXS=0.176*(TC/((MW*1E+3)**3*(PC/1E+5)**4))**(1./6)! INVERSE VISCOSITY
VISD=ETAEX*1E-7/EXS      ! DYNAMIC VISCOSITY, [Pa-s]
VIS=VISD/DENS            ! KINEMATIC VISCOSITY, [m^2/s]

! ESTIMATION OF THERMAL CONDUCTIVITY
! EQS. (10-5.2, 3, 4), PAGE 10.22 OF POLING ET AL. (2001)

KO=18.006E-3            ! THERMAL CONDUCTIVITY AT LOW PRESSURE
GAM=210*(TC*(MW*1E+3)**3/(PC/1E+5)**4)**(1./6)! INV. THERMAL COND.
VOL= ZV*R*TA/P          ! VOLUME, [m^3/mol]
!DENR=VC/VOL            ! REDUCED DENSITY
DENR=3.*P*TC/8./ZV/TA/PC

IF (DENR.LT.0.5) THEN
K=1.22E-2*(EXP(0.535*DENR)-1.0)/(GAM*ZC**5)+KO !THERMAL COND., [W/m-K]
ELSE IF (DENR.LT.2.0) THEN
K=1.14E-2*(EXP(0.67*DENR)-1.069)/(GAM*ZC**5)+KO
ELSE
K=2.60E-3*(EXP(1.155*DENR)+2.016)/(GAM*ZC**5)+KO
END IF

! CALCULATION OF PLATE LENGTH FOR LAMINAR FLOW

BETAR=1./TA
PR=VISD*CP/K          ! PRANDLT NUMBER
DL=(1.05E+9*VIS**2/(BETAR*GR*(TW-TF)*PR))**(1./3)! LENGTH OF THE PLATE, [m]
WRITE(*,*)DL

! DIMENSIONLESS PARAMETERS

GRL=BETAR*GR*(TW-TF)*DL**3/(VIS**2)      ! GRASHOF NUMBER
G=BETAR*GR*(TW-TF)*(W**4)/((VIS**2)*DL) ! DIMENSIONLESS COEFFICIENT
RAL=GRL*PR                                ! RAYLEIGH NUMBER
XMAX=1./G                                  ! DIMENSIONLESS DOMAIN LENGTH
WRITE(*,*)G,XMAX,TW,TF,TA,BETAR

REX=0.2                                    ! UNDERRELAXATION FACTOR

WRITE(*,*)'Grashof=',GRL,' Prandtl=',PR,' Rayleigh=',RAL
WRITE(*,*)'DENS=',DENS,' CP=',CP,' VISD=',VISD,' VIS=',VIS,' K=',K

```

```
!WRITE(*,*)ZL,ZV
```

```
CALL CALCBETA(P,TW,PC,TC,BETA)
```

```
BET(1)=BETA
BETD(1)=BETA/BETAR
```

```
X = 0.0
```

```
SUM=0
NUMP=100
```

```
DO IT=1,NUMP
    SUM=SUM+1.05**IT
END DO
```

```
DX =0.75*XMAX/SUM
DXMAX=DX*(1.05**NUMP)
```

```
II=1
N = 300
Y(1) = 0.0
DY = 1./N !DY=W/N
```

```
DO J = 2,N
    Y(J) = Y(J-1) + DY
END DO
```

```
!***** ASSIGN INITIAL VALUES *****
```

```
U(1,1) = 0.0
V(1,1) = 0.0
T(1,1) = 1.0
```

```
DO J = 2,N
    U(1,J) = 0.0
    T(1,J) = 0.0
    V(1,J) = 0.0
```

```
END DO
```

```

!*****
!           PROCESSING: KERNEL ALGORITHM
!*****

! SOLUTION BEGINS

      NX=0

      DO WHILE (X.LT.XMAX)

          NX=NX+1
          ITER=0
          VCHX=0.0

          DO J = 1,N

              U(2,J) = U(1,J)
              T(2,J) = T(1,J)
              V(2,J) = V(1,J)

          END DO

          IF(DX.LT.DXMAX) THEN
              DX=1.05*DX
          ELSE
              DX=DXMAX
          END IF

          X = X + DX

          V(2,1) = 0.0
          U(2,1) = 0.0
          T(2,N) = 0.0
          T(2,1) = 1.0

          DO NIT=1,100

              ITER=ITER+1

!***** SOLVE ENERGY EQUATION TO GET "T" *****

              A(1)=1.0
              B(1)=0.0
              C(1)=0.0
              D(1)=T(2,1)

              DO J = 2,N

                  A(J) = (2.0/(DY*DY*PR))+U(2,J)/DX
                  B(J) = V(1,J)/(2.0*DY)-1.0/(DY*DY*PR)

```

$$C(J) = -V(1,J)/(2.0*DY)-1.0/(DY*DY*PR)$$

$$D(J) = U(2,J)*T(1,J)/DX$$

END DO

A(N)=1.0  
 B(N)=0.0  
 C(N)=0.0  
 D(N)=0.0

CALL TRISOL(N,A,B,C,D,H)

DO J = 1,N

$$T(2,J) = T(2,J)+REX*(H(J)-T(2,J))$$

END DO

!\*\*\*\*\* SOLVE MOMENTUM EQUATION TO GET "U" \*\*\*\*\*

A(1)=1.0  
 B(1)=0.0  
 C(1)=0.0  
 D(1)=0.0

DO J = 2,N

$$TEMP1 = T(2,J)*(TW-TF)+TF$$

CALL CALCBETA(P,TEMP1,PC,TC,BETA)

BET(J)=BETA  
 BETAD=BETA/BETAR  
 BETD(J)=BETAD

$$A(J) = (2.0/(DY*DY))+U(2,J)/DX$$

$$B(J) = V(2,J)/(2.0*DY)-1.0/(DY*DY)$$

$$C(J) = -V(2,J)/(2.0*DY)-1.0/(DY*DY)$$

$$D(J) = U(2,J)*U(1,J)/DX+BETAD*T(2,J)$$

END DO

A(N)=1.0  
 B(N)=0.0  
 C(N)=0.0  
 D(N)=0.0

CALL TRISOL(N,A,B,C,D,H)

DO J = 1,N

```

                U(2,J) = U(2,J)+REX*(H(J)-U(2,J))
            END DO

!***** SOLVE THE CONTINUITY EQUATION TO GET "V" *****

                DO J = 2, N
                V(2,J) = V(2,J-1)-(DY/(2.0*DX))*(U(2,J)-U(1,J)+U(2,J-1)-U(1,J-1))
                END DO

!***** CHECK CONVERGENCE *****

                VDIFF=ABS(V(2,N)-VCHX)
                IF(VDIFF.LE.0.01) EXIT
                VCHX=V(2,N)
            END DO

! ***** SAVING DATA *****

                II=II+1

                DO J=2,N

                    XX(II)=X
                    VELU(II,J)=U(2,J)
                    VELV(II,J)=V(2,J)
                    TEMP(II,J)=T(2,J)

                END DO

! ***** RETURN VALUES *****

                DO J=1,N
                    U(1,J)=U(2,J)
                    V(1,J)=V(2,J)
                    T(1,J)=T(2,J)
                END DO
            END DO
            WRITE(*,*)NX,ITER

!*****

!               POST-PROCESSING: PRINTING THE RESULTS

!*****

! RESULTS IN THE DIMENSIONLESS DOMAIN

                WRITE (8,*) "TITLE="TEMPERATURE FIELD"
                WRITE (8,*) "VARIABLES = "Y", "X", "VELV", "VELU", "TEMPERATURE"
                WRITE (8,*) "ZONE T="ZONE001", I=', II, ' J=', N, ' F=BLOCK'
                WRITE (1,35) 'DIMENSIONLESS VALUES'

```

```

WRITE (1,*) ''
WRITE (1,40) 'Y', 'U', 'V', 'T', 'BETAD'
WRITE (1,*) ''

XX(1)=0.0

DO J = 1,N
    VELU(1,J)=0.0
    VELV(1,J)=0.0
    TEMP(1,J)=0.0

END DO

DO I = 1,II
    TEMP(I,1)=1.0
END DO

DO J=1,N
    WRITE(8,25) (Y(J),I=1,II)
END DO

DO J=1,N
    WRITE(8,25) (XX(I),I=1,II)
END DO

DO J=1,N
    WRITE(8,25) (VELV(I,J),I=1,II)
END DO

DO J=1,N
    WRITE(8,25) (VELU(I,J),I=1,II)
END DO

DO J=1,N
    WRITE(8,25) (TEMP(I,J),I=1,II)
END DO

DO J=1,N
    WRITE(1,30)Y(J),VELU(100,J),VELV(100,J),TEMP(100,J),BETD(J)
END DO

CLOSE(1)

```

! \*\*\*\*\* RESULTS IN THE DIMENSIONAL DOMAIN \*\*\*\*\*

```

WRITE (9,*) 'TITLE="TEMPERATURE FIELD"'
WRITE (9,*) 'VARIABLES = "Y", "X", "VELV", "VELU", "TEMPERATURE"'
WRITE (9,*) 'ZONE T="ZONE001", I=, II, ' J=, N, ' F=BLOCK'
WRITE (2,45)'DIMENSIONAL VALUES'
WRITE (2,*) ''
WRITE (2,50) 'y', 'u', 'v', 'T', 'BETA','BETAR'
WRITE (2,*) ''

```

```

WRITE (3,55) 'x','T','h','Nu','Ra'
WRITE (3,*) ''

XX(1)=0.0

DO J = 1,N
    VELU(1,J)=0.0
    VELV(1,J)=0.0
    TEMP(1,J)=0.0
!
END DO

DO I = 1,II
    TEMP(I,1)=1.0
END DO

! RETURNING TO THE DIMENSIONAL DOMAIN

DO I = 1,II
    XX(I)=XX(I)*DL*G
END DO

DO J = 1,N
    Y(J)=Y(J)*W
END DO

DO J = 1,N
    DO I = 1,II
        VELU(I,J)=VELU(I,J)*VIS*DL*G/(W**2)
        VELV(I,J)=VELV(I,J)*VIS/W
        TEMP(I,J)=TEMP(I,J)*(TW-TF)+TF
    END DO
END DO

! CONVECTIVE COEFFICIENT, [W/m^2·K]

DO I=1,II
    COEF(I)=-K*(TEMP(I,2)-TW)/(DY*W*(TW-TF))
END DO

! NUSSELT NUMBER

DO I=1,II
    NU(I)=COEF(I)*XX(I)/K
END DO

! GRASHOF NUMBER

DO I=1,II
    GRX(I)=BETAR*GR*(TW-TF)*XX(I)**3/VIS**2
END DO

```

! RAYLEIGH NUMBER

```
DO I=1,II
  RAX(I)= GRX(I)*PR
END DO
```

! AVERAGE CONVECTIVE COEFFICIENT

S=0

```
DO I=1,II-1
  S=S+(COEF(I+1)+COEF(I))*(XX(I+1)-XX(I))/2
END DO
```

COEFP=S/DL

! AVERAGE NUSSELT NUMBER

NUP=COEFP\*DL/K

```
DO J=1,N
  WRITE(9,25) (Y(J),I=1,II)
END DO
```

```
DO J=1,N
  WRITE(9,25) (XX(I),I=1,II)
END DO
```

```
DO J=1,N
  WRITE(9,25) (VELV(I,J),I=1,II)
END DO
```

```
DO J=1,N
  WRITE(9,25) (VELU(I,J),I=1,II)
END DO
```

```
DO J=1,N
  WRITE(9,25) (TEMP(I,J),I=1,II)
END DO
```

```
DO J=1,N
WRITE(2,30)Y(J),VELU(100,J),VELV(100,J),TEMP(100,J),BET(J),BETAR
END DO
```

```
DO I=1,II
  WRITE(3,31)XX(I),TEMP(I,2),COEF(I),NU(I),RAX(I)
END DO
```

```

WRITE(3,*)' '
WRITE(3,*)'AVERAGE CONVECTIVE COEFFICIENT'
WRITE(3,*)COEFP
WRITE(3,*)'AVERAGE NUSSELT NUMBER'
WRITE(3,*)NUP

25 FORMAT (1X,300F15.5)
30 FORMAT (6E15.6)
31 FORMAT (5E15.6)
35 FORMAT (25X,A20)
40 FORMAT (9X,A1,14X,A1,14X,A1,14X,A1,12X,A5)
45 FORMAT (25X,A18)
50 FORMAT (9X,A1,14X,A1,14X,A1,14X,A1,14X,A4,10X,A5)
55 FORMAT (9X,A1,14X,A1,14X,A1,14X,A2,14X,A2)

STOP
CLOSE(2)
END

!*****

SUBROUTINE TRISOL(NN,A,B,C,D,H)

!***** THIS IS A TRI-DIAGONAL MATRIX SOLVER *****

! THIS TRIDIAGONAL MATRIX SOLVER USES THE THOMAS ALGORITHM

DIMENSION A(300),B(300),C(300),D(300),H(300),W(300),Q(300),G(300)

W(1)=A(1)
G(1)=D(1)/W(1)

DO K=2,NN
  K1=K-1
  Q(K1)=B(K1)/W(K1)
  W(K)=A(K)-C(K)*Q(K1)
  G(K)=(D(K)-C(K)*G(K1))/W(K)
END DO

H(NN)=G(NN)
N1=NN-1

DO K=1,N1
  KK=NN-K
  H(KK)=G(KK)-Q(KK)*H(KK+1)
END DO

RETURN
END

```

```

!*****
SUBROUTINE ZETA(P,T,PC,TC,ZV,ZL,IROOT)

!***** THIS IS TO COMPUTE COMPRESSIBILITY FACTOR *****

DOUBLE PRECISION ARG, QQ, RR, DD
COMMON IONE,ITHREE
PI=3.14159          ! PI IN RADIANS

! DIMENSIONALESS VARIABLES

TRED=T/TC          ! REDUCED TEMPERATURE
PRED=P/PC          ! REDUCED PRESSURE

A=(27./64)*(PRED/TRED**2)
B=(1./8)*(PRED/TRED)

! SOLVING POLINOMIAL EQUATION OF THE FORM: Z**3+P1*Z**2+P2*Z+P3=0

P1=-B-1
P2=A
P3=-A*B

QQ=(3*P2-P1**2)/9
RR=(9*P1*P2-27*P3-2*P1**3)/54
DD=QQ**3+RR**2          !DISCRIMINANT

IF(DD.GE.0) THEN
  BASE=RR+SQRT(DD)
  SS=SIGN((ABS(BASE))**(1./3),BASE)

  BASE=RR-SQRT(DD)
  TT=SIGN((ABS(BASE))**(1./3),BASE)

  ZV=SS+TT-(1./3)*P1
  ZL=ZV

  IROOT=1
  IONE=IONE+1
ELSE
  ARG=RR/DSQRT((-QQ)**3)
  ALPHA=ACOS(ARG)
  RQ=SQRT(-QQ)
  Z1=2*RQ*COS(ALPHA/3)-(1./3)*P1
  Z2=2*RQ*COS(ALPHA/3+2*(PI/3))-(1./3)*P1
  Z3=2*RQ*COS(ALPHA/3+4*(PI/3))-(1./3)*P1
  ZL=MIN(Z1,Z2,Z3)
  ZV=MAX(Z1,Z2,Z3)
  IROOT=3
  ITHREE=ITHREE+1

```

```

END IF
RETURN
END

```

```

!*****

```

```

SUBROUTINE CALCBETA(P,T,PC,TC,BETA)

```

```

!***** THIS IS TO COMPUTE BETA *****

```

```

COMMON IONE,ITHREE
CALL ZETA(P,T,PC,TC,ZV,ZL,IROOT)

```

```

Z=ZL

```

```

! DIMENSIONALESS VARIABLES

```

```

TRED=T/TC          ! REDUCED TEMPERATURE
PRED=P/PC          ! REDUCED PRESSURE

```

```

A=(27./64)*(PRED/TRED**2)
B=(1./8)*(PRED/TRED)

```

```

FZ=1-(Z**2*B-2*A*Z+3*A*B)/(3*Z**3-2*Z**2*(B+1)+Z*A)
BETA=FZ/T

```

```

RETURN
END

```